AD-A081 946 GEORGIA INST OF TECH ATLANTA SCHOOL OF PHYSICS F/G 7/4
ELECTRONIC EXCITATION STRUCTURE, CORRELATION, AND RELAXATION AN--ETC(U)
NOV 79 M W RIBARSKY AFOSR-76-3108

UNCLASSIFIED AFOSR-TR-80-0202 NL

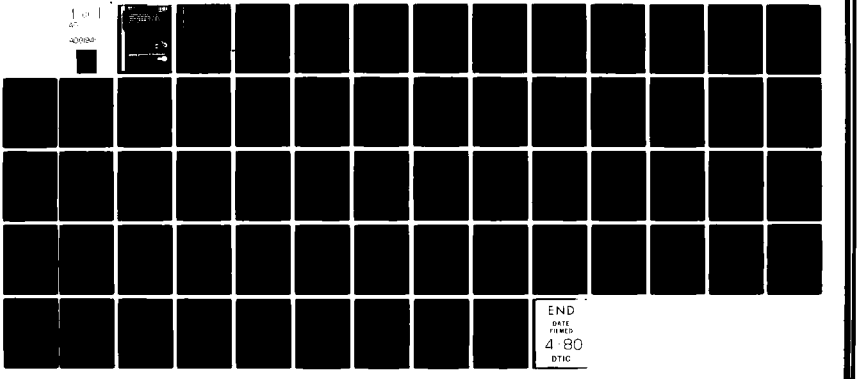

END
DATE FILMED
4-80
DTIC

UNCLASSIFIED

SECURITY CLASSIFICATION OF THIS PAGE (When Data Entered)

REPORT DOCUMENTATION PAGE	READ INSTRUCTIONS BEFORE COMPLETING FORM
1. REPORT NUMBER (19) (18) AFOSR-TR- 80-0202 / 2. GOVT ACCESSION NO.	3. RECIPIENT'S CATALOG NUMBER
4. TITLE (and Subtitle) (1) Electronic Excitation Structure, Correlation, and Relaxation and Their Effects on the Optical Properties and Electron Emission of Transition Metal Oxides	5. TYPE OF REPORT & PERIOD COVERED FINAL Oct. 1, 1976 to Sept. 30, 1979
	6. PERFORMING ORG. REPORT NUMBER
7. AUTHOR(s) (10) M. W. Ribarsky	8. CONTRACT OR GRANT NUMBER(s) (15) AFOSR-76-3108
9. PERFORMING ORGANIZATION NAME AND ADDRESS Georgia Institute of Technology School of Physics Atlanta, Ga. 30332 (17) A5	10. PROGRAM ELEMENT, PROJECT, TASK AREA & WORK UNIT NUMBERS 61102F 2301 A5 (16)
11. CONTROLLING OFFICE NAME AND ADDRESS AIR FORCE OFFICE OF SCIENTIFIC RESEARCH/NP BOLLING AFB, BUILDING 410 WASHINGTON, DC 20332	12. REPORT DATE Nov. 30, 1979
	13. NUMBER OF PAGES 60
14. MONITORING AGENCY NAME & ADDRESS (if different from Controlling Office) (9) Final rept 1 Oct 76-30 Sep 79	15. SECURITY CLASS. (of this report) unclassified
	15a. DECLASSIFICATION/DOWNGRADING SCHEDULE
16. DISTRIBUTION STATEMENT (of this Report) APPROVED FOR PUBLIC RELEASE, DISTRIBUTION UNLIMITED (12) 63	
17. DISTRIBUTION STATEMENT (of the abstract entered in Block 20, if different from Report) (11) 30 Nov 79	
18. SUPPLEMENTARY NOTES	
19. KEY WORDS (Continue on reverse side if necessary and identify by block number) OPTICAL PROPERTIES, TRANSITION METAL OXIDES, BAND STRUCTURE, CORRELATION	

20. ABSTRACT (Continue on reverse side if necessary and identify by block number)

Studies of the electronic excitation structure of transition metal oxides and the effect of the structure on the optical properties, electron correlations, and photoemission spectra of these materials have been made. Techniques have been developed which for the first time allow precise and general calculations of the excitation structure so that in addition to the above properties several other properties can be obtained. These techniques have been applied in particular to calculations on TiO. The calculations allow comparison with

DD FORM 1 JAN 73 1473 EDITION OF 1 NOV 65 IS OBSOLETE UNCLASSIFIED 404237

SECURITY CLASSIFICATION OF THIS PAGE (When Data Entered)

experiment and identification of the structure in the optical spectra of oxidized surfaces. They also show that significant correlation and relaxation effects occur in the band structure.

ELECTRONIC EXCITATION STRUCTURE, CORRELATION, AND RELAXATION AND THEIR EFFECTS ON THE OPTICAL PROPERTIES AND ELECTRON EMISSION OF TRANSITION METAL OXIDES

Final Scientific Report

Electronic Excitation Structure, Correlation, and Relaxation and their Effects on the Optical Properties and Electron Emission of Transition Metal Oxides

By

M. W. Ribarsky

November 30, 1979

Grand No. AFOSR-76-3108

TABLE OF CONTENTS

I. INTRODUCTION

A system responds to an external probe by undergoing various excitations in order to distribute the energy and momentum transferred from the probe. The nature of these excitations, their characteristic energies and distributions, establishes the properties of the system. Thus the electronic excitation structure of a system establishes its optical and electrical properties and the pattern of its electronic emission.

An understanding of the electronic excitation structure elucidates experimental methods which probe the optical properties, the electron emission and energy loss spectra and the collective excitation modes of a system. Advancing in an interlocking manner, the experimental methods, which are now providing a wealth of precise data, then give an even more refined interpretation of the theory which can be revised and tested anew. Moreover, when the relationship between experiment and theory is understood, experiment can be used to show the effect of changes in the basic electronic properties and other properties not included in the theory. For example, the probe of oxides grown an titanium with reflectivity and Auger measurements yields information on the basic electronic structure of the oxide which can be related to changes which also occur in the electrical conductivity and growth rate of the oxide.

In this work a dielectric response theory has been formulated to describe the electronic excitation structure of a solid state system. The properties and experimental methods mentioned above can be investigated within the framework of this theory. In addition one can look at electronic correlations which can produce large collective modes such as plasmons or which can have profound effects on the band structure of the system.

We have used the local orbitals technique in constructing the dielectric response. This framework allows the wedding of ground state calculations of energy

bands and wavefunction with excitation calculation in the same representation, and it is especially well suited for materials with narrow d-bands. With the local orbitals technique, we can calculate symmetry-breaking, localized excitations more easily. The dielectric response model then allows the inclusion of both the symmetric-state ground and the symmetry-broken excited state and permits the calculation of the excitation energy and transition rate in one step.

We have concentrated on the properties of transition metal oxides in this work. The partially filled d-bands are the distinguishing feature of transition metal chemistry. These bands are relatively narrow, but they are overlapped by the next higher s-band causing a great deal of s-d hybridization. On the other hand in some transition metal compounds, such as many of the oxides, the bonds are mostly ionic and the highest metallic s-band is unoccupied. In this case the highest s-band moves away from the partially filled d-band. Then the s-d hybridization is much less and the d-band is quite narrow. Quantitative knowledge of the degree of hybridization of these bands and the related structure of the bonds in the solid is very important for understanding many mechanisms such as electrical conductivity and catalysis. Since many of the oxides of the transition metals, especially titanium, exist in several structures with widely different electrical properties, this knowledge also enables us to identify the oxides occuring on transition metals by analyzing, for example, optical absorption spectra. Evidently, the electronic structure of these oxides is related to the rate of oxidation of the transition metal and to its degree of corrosion.

II. OBJECTIVES

The purpose of this research was to formulate and implement a dielectric response method for calculating excitation structure and to apply the method to calculations of the electronic properties of transition metal oxides. Important initial objectives were to set up a dielectric response theory in the framework of the local orbitals technique and to devise methods for calculating the excitation structure. This latter objective was not easily realized since it required very efficient techniques to handle large matrices and to calculate and sort large numbers of multicenter two electron integrals. The next objective was to focus on transition metal oxides, especially TiO. The properties of these materials were analyzed with emphasis on the optical properties. Experimental results were viewed in the light of this analysis, and several properties of the oxide system under different conditions of oxidation were elucidated. A final objective was the study of several materials to get an idea of the range of excitation structures and the wide variation of electronic properties.

III. ACHIEVEMENTS

A. Development of Dielectric Response Theory in Local Orbitals Framework.

The central point of any local orbitals expansion is that the charge density may be written as

$$\rho(\vec{r},\vec{r}') = \sum_{\substack{ij \\ a,b}} \phi_{ai}(\vec{r})\, T_{ai,bj}\, \phi^{*}_{bj}(\vec{r}') \qquad (1)$$

where

$$\phi_{ai}(\vec{r}) = \phi_{i}(r-\vec{R}a),$$

and ϕ_{ai} is localized in space. The matrix T contains the coefficients for the Bloch states in terms of linear combinations of the ϕ's. A particular choice of ϕ occurs when one rotates in the subspace of occupied Bloch states. This rotation leaves ρ in Eq. (1) unchanged, but allows one to solve for it in a new set of equations

$$(F(\rho) + \rho A \rho)\,|\phi_{ai}\rangle = E_{ai}\,|\phi_{ai}\rangle \qquad (2)$$

where F is the Fock operator and A is an arbitrary Hermitian operator chosen such that ϕ_{ai} is well-localized. This is the "local orbitals methods" of Kunz[1], the results of which we have used extensively in this work.

One may use the field-theoretic methods to contruct the particle hole (PH) polarization propagator $\underline{\Pi}(\omega)$, the poles of which are the excitation energies. Under certain assumptions,[2] the equation for $\underline{\Pi}(\omega)$ reduces to a Dyson-like equation

$$\underline{\Pi}(\omega)^{-1}\,\vec{C}(\omega) = \Lambda(\omega)\,\vec{C}(\omega) \qquad (3)$$

with

$$\underline{\Pi}(\omega)^{-1} = \underline{\Pi}^{0}(\omega)^{-1} - \underline{K}(\omega) \qquad (4)$$

The kernel $\underline{K}(\omega)$ contains two electron matrix elements describing the particle-hole interactions. $\underline{\Pi}^{o}(\omega)$ is the zero'th order PH propagator (without particle-hole interactions) and thus is constructed wholly with ground state energy bands and wave functions. One solves Eq. (3) for the values $\omega = \omega_n$ for which $\Lambda(\omega)=0$. These are the excitation energies of the crystal. Then $\Pi(\omega)$ is

$$\Pi_{ss'}(\omega) = \sum_n \left[\frac{c_s^n(\omega) c_{s'}(\omega)^+}{\omega-\omega_n(\omega)+i\eta} - \frac{c_{s'}^n(\omega) c_s^n(\omega)^+}{\omega-\omega_n(\omega)-i\eta} \right] \qquad (5)$$

where $\eta = 0^+$. In the random phase approximation (RPA),[2] $\underline{K}(\omega)$ does not depend on ω so that C_s^n and ω_n are independent of ω. Then the solution of Eq. (3) is much simplified as we will show below.

The difficulty in solving Eq. (6) for crystalline systems is that $\underline{\Pi}(\omega)^{-1}$ is not block diagonal in momentum as is the Fock operator, for example. It depends on the initial momentum $\vec{k}$ and on the momentum transfer between ground and excited state $\vec{q}$. Thus $\underline{\Pi}$ has off-diagonal elements in momentum which give rise to "local field effects". These effects are related to the formation of a "localized hole" upon excitation, for if the hole were delocalized, the excited state would have the full symmetry of the ground state and $\underline{\Pi}(\omega)$ would be diagonal. Thus when local field effects are present, one must diagonalize a huge matrix in momentum space. On the other hand, if instead of momentum a sufficiently localized representation such as Wannier functions were used, one could diagonalize $\underline{\Pi}(\omega)^{-1}$ in a manageable subspace.

We can avoid the difficulties of the Bloch representation by transforming to a local orbitals basis. The transformation requires a matrix $T_s(k_1 k_2)$ which contains all the coefficients for a local orbitals expansion of the Bloch functions where S is a condensed notation for the local orbitals indices, and k_1/k_2 are

are condensed notations for the initial/final Bloch states. Then

$$\Pi^{o}_{ss'}(q,\omega)^{-1} = \sum_{k_1 k_2} T_s^{*}(\vec{k}_1,\vec{k}_2+\vec{q})\ \chi^{o}(\vec{k}_1,\vec{k}_2+\vec{q}\ ;\omega)^{-1}\ T_{s'}(\vec{k}_1,\vec{k}_2+\vec{q}) \quad (6)$$

χ_o^{-1} is just the inverse of the polarizability for the non-interacting electron-hole pair[3], and it is given by

$$\chi^{o}(\vec{k}_1,\vec{k}_2+\vec{q};\omega) = F_{\vec{k}_1}(1-F_{\vec{k}_2+\vec{q}})\ \{\omega-E_{\vec{k}_2+\vec{q}} + E_{\vec{k}_1}\} \quad (7)$$

$$- F_{\vec{k}_2+\vec{q}}\ (1-F_{\vec{k}_1})\ \{\omega + E_{\vec{k}_2+\vec{q}} - E_{\vec{k}_1}\}$$

where $E_{\vec{k}}$ and $F_{\vec{k}}$ are the one-particle energy and occupation number for Bloch state $\vec{k}$. The inclusion of $\underline{K}$ in Eq. (4) introduces particle-hole interaction effects. In the RPA, $\underline{K}$ is

$$K_{ss'} = V_{ai\ bj,\ b'j'a'i'} - V_{ai\ a'i',b'j'bj}$$
$$V_{aibj,b'j'a'i'} \equiv \langle \phi_{ai}(\vec{r})\phi_{b'j'}(r')\ \frac{e^2}{|\vec{r}-\vec{r}'|}\ \phi_{bj}(\vec{r})\phi_{a'i'}(\vec{r}')\rangle . \quad (8)$$

The set of equations (3-8) constitute a system to find the energies and transition rates for excitations from the self-consistent ground state of the crystalline solid. A much smaller subspace of local orbitals is needed for these equations than would be necessary using Bloch functions. In addition the calculation is based on the fully self-consistent ground state band structure of the system: this is the first time such a calculation has been done. Hanke and Sham[4] have used a similar set of equations in model calculations on diamond. However they directly invert $\underline{\Pi}(\omega)^{-1}$ in Eq. (4) for each ω; such an approach would be

prohibitively time-consuming for a full calculation. As we will show below, it is possible to diagonalize Eq. (3) and get a complete spectrum in one step.

To proceed we may decompose Eq. (6) using Eq. (7) thusly

$$\Pi^{o}_{ss'}(\vec{q},\omega)^{-1} = \omega\, O_{ss'}(\vec{q}) - W_{ss'}(\vec{q}) \tag{9}$$

where

$$O_{ss'}(\vec{q}) = \sum_{k_1 k_2} T_s^{*}(\vec{k}_1,\vec{k}_2+q)\ (F_{k_1}-F_{\vec{k}_2+\vec{q}})\ T_{s'}(\vec{k}_1,\vec{k}_2+\vec{g}) \tag{10}$$

$$W_{ss'}(\vec{q}) = \sum_{k_1 k_2} T_s^{*}(\vec{k}_1,\vec{k}_2+\vec{q})\Big[(F_{k_1} + F_{\vec{k}_2+\vec{q}} - 2F_{k_1}F_{\vec{k}_2+\vec{q}}) \times (E_{\vec{k}_2+\vec{q}} - E_{k_1})\Big]\, T_{s'}(\vec{k}_1,\vec{k}_2+\vec{q}). \tag{11}$$

$\underline{O}(\vec{q})$ in Eq. (10) behaves like an overlap matrix in that it is positive definite. Then we can write

$$O(\vec{q}) = \underline{L}(\vec{q})L^{+}(q) \tag{12}$$

so that for $\Lambda = 0$ and after transformation, Eq. (3) becomes

$$\omega_n(\vec{q})\vec{C}^{n'}(\vec{q}) = \left[\underline{W}'(\vec{q}) - \underline{K}'(\vec{q})\right]\vec{C}^{n'}(\vec{q}) \tag{13}$$

with

$$\underline{W}'(\vec{q}) = \underline{L}^{-1}(\vec{q})\underline{W}(\vec{q})(\underline{L}^{+}(\vec{q})^{-1}$$

and so on. The nature of the transformation ensures that the matrices in Eq. (13) remain Hermitian. We can therefore treat Eq. (13) as an eigenvalue problem and

diagonalize to find the spectrum ω_n for each $\vec{q}$. For the optical spectrum, we may treat the limit $\vec{q} \to 0$ and diagonalize Eq. (13) only once. However, for problem such as correlation, a smapling for $\vec{q}$ throughout the Brillouin Zone must be made.

B. Devising Methods of Calculation.

It turns out that the solution of Eq. (13) is no easy matter because of the size and complexity of the matrices involved and because of the need to calculate multicenter integrals. We discuss some of the methods used on this problem in more detail in this section because they represent achievements of wider applicability than just to the present problem.

As presented in Eq. (8), the kernel $\underline{K}$ depends on individual multicenter two electron integrals. Two problems exist with the calculation of $\underline{K}$. The first is that the multicenter integrals can be difficult and time-consuming to calculate. In fact, if one uses Slater type orbitals (STO's) the integral expression does not have a closed form and one must do an expansion over angular momentum states, the sum becoming more complicated for three - and four - center integrals. The second problem is that the integrals do not sum nicely into a quantity, like the Fock matrix in Hartree Fock calculations, which has the initial symmetry of the system. This happens because the excited system no longer depends on just the one-electron density matrix and completely breaks symmetry in general. Thus the sorting of the integral labels is a major accounting problem. We have found quite effective methods for solving both these problems in the Unrestricted Hartree Fock (UHF) molecular cluster codes developed by Robert Euwema and Frank Tobin under an Air Force grant. Frank Tobin has consulted with us and helped us to understand the methods used in the UHF code. He has also helped us to maintain the code in running order, and we are using it for several other calculations.

Initially, since our original local orbitals were in STO's, we calculated our multicenter integrals in terms of STO's. We devised a set of codes which would calculate integrals for states of any angular momentum on any set of sites. These codes will be useful for limited calculations in the future (for example, calculations involving high angular momentum states), but they proved too slow for the excitation calculations. However, the UHF code has the most efficient multicenter integrals package currently available for calculations involving s,p, or d symmetries, and we were able to modify the package for our purposes. This code calculates integrals in terms of Gaussian type orbitals (GTO's), and the integrals can be calculated without an expansion in terms of angular momentum states. The extra effort necessary to expand the individual STO's in terms of GTO's was worth paying in return for the much quicker integral generation.

The sorting of the integrals labels was complicated by the fact that some of the lattice vector indices must be summed over, for example, in the optical absorption calculation before the final sort can be done. Luckily, the UHF package has a remarkable general code based on the Yoshimine procedure which allows the sorting of labels initially in any order. We were able to adapt this code to our purposes.

After the matrices are finally constructed, we face the problem of diagonalizing them. Actually, two diagonalizations must be done on large matrices of somewhat different character. The matrices are large because two sets of indices are needed, one set for the initial electron and one for the final state, and because the lattice vector must also be indexed. In general, all the indices appearing on the RHS of Eq. (8) explicitly appear in the matrix. For our calculation on TiO, where it was only necessary to use the valence p and d local orbitals and up to the next nearest neighbor lattice vectors, the dimensions of the matrices were still 622 x 622. For a complex, Hermitian matrix of this size,

standard diagonalization techniques would take about three hours of computer time to find all the eigenvalues and eigenvectors. We devised a scheme involving diagonalization of sub-blocks within the matrix and then correcting them perturbatively which markedly reduced the computation time.

The matrix $\underline{0}$ in Eq. (10) is dense and does not easily separate into blocks. However it is diagonally dominant and blocking tendencies are apparent. To illustrate the procedures used, in Fig. 1 we show density maps of a 150 x 150 sub-block of our large matrix. Each symbol in the maps represents an average magnitude of the elements in the small block at that position, the larger magnitude elements being represented by darker, built-up symbols. The blank areas in the maps contain non-zero elements which are below a given tolerance in magnitude. Thus the map is a display of the distribution of magnitudes of matrix elements. The first step is to take the original matrix in Fig. 1a and interchange rows and columms so that the diagonal elements are ordered in magnitude. As shown in Fig 1b, this step greatly condenses the density pattern. We then choose blocks along the diagonal (in this case four are chosen) so that the natural blocking pattern displayed by the map is followed, and we find the eigenvalues and eigenvectors of each block. We perform the unitary transformation using the block diagonal matrix composed of the eigenvectors with the result in Fig. 1c. Now the diagonal blocks just have eigenvalues in descending order on the diagonal with zeros on either side, and the off-diagonal blocks <u>also</u> have a particular order. The matrix is now ready for further rearrangement. One possiblility is shown in Fig 1d where we have simply sorted the diagonal elements again as we did in Fig. 1b. The solutions are finally corrected perturbatively as outlined below. Before the perturbation corrections is attempted, however, eigenvalues which are very close or which are connected by large off-diagonal matrix elements must be blocked together since they will make the perturbation expansion unstable.

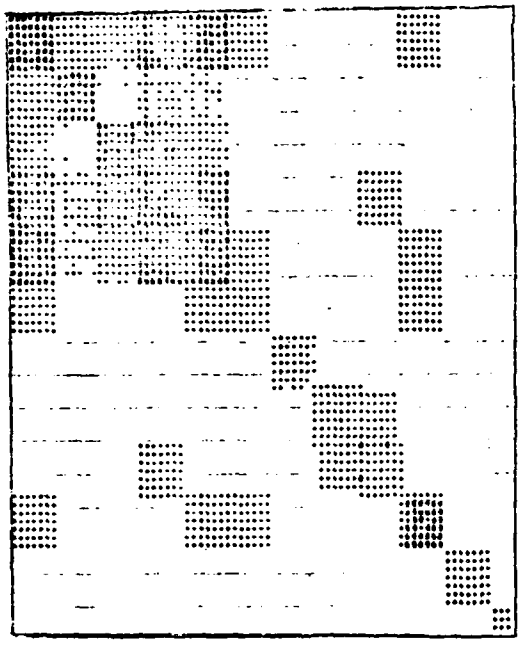

(a)

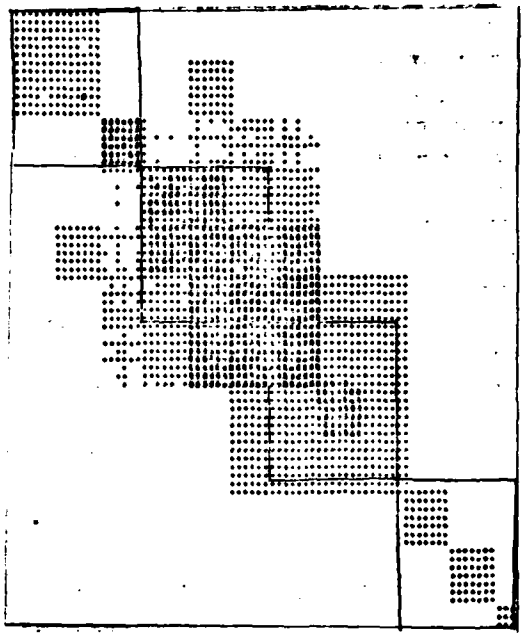

(b)

Fig. 1 Example of matrix rearrangement and sub-block diagonalization.

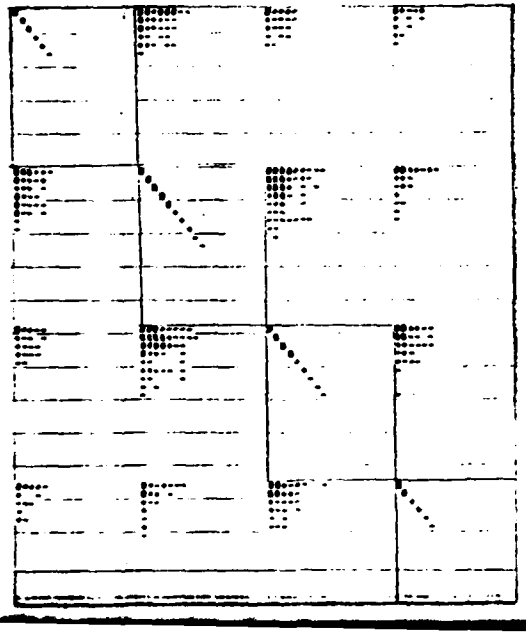

(c)

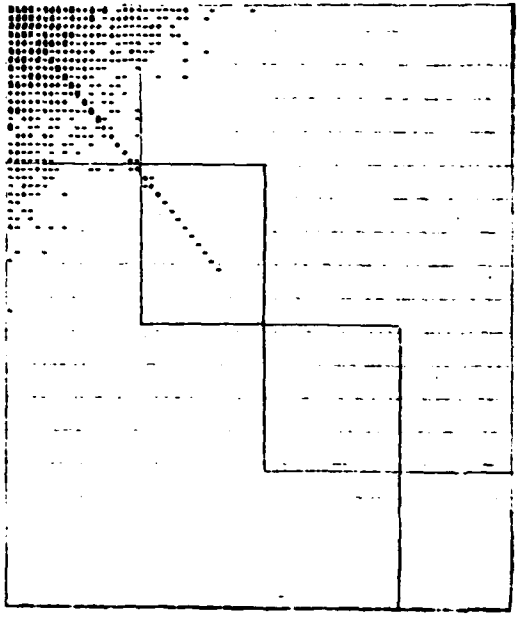

(d)

For optimally blocked matrices two diagonalizations of sub-blocks followed by perturbative corrections give good results. For diagonalizing any large, non-sparse matrix, a topic which has not received much attention, these procedures are useful.

The matrix $\underline{W}'(q)-\underline{K}'(q)$ in Eq. (13) is also dense, but it blocks more easily owing to the contributions of the two electron terms in $\underline{K}'(q)$. We can diagonalize each of these blocks separately, and then, using a variation on degenerate perturbation theory, we can include the effects of terms not in the blocks. Let us assume we want to block diagonalize the matrix $\underline{\Pi}(\omega)^{-1}$ which is arranged as in Fig. 2. We have assumed the total matrix is of size Nm x Nm and have arranged the elements along the diagonal into Nmxm blocks, $\underline{\Pi}_{11}^{-1}.....\underline{\Pi}_{nn}^{-1}$, although there is no need to restrict ourselves to blocks of equal size. Then the eigenvalue problem becomes

$$(\Delta-\underline{\Pi}_{11}^{-1})\vec{C}_1 = \sum_{\mu\neq 1} \underline{\Pi}_{1\mu}^{-1}(\Delta-\underline{\Pi}_{\mu\mu}^{-1})^{-1}\underline{\Pi}_{\mu 1}^{-1}\vec{C}_1 \qquad (14)$$

$$+ \sum_{\mu\neq\nu\neq 1} \underline{\Pi}_{1\mu}^{-1}(\Delta-\underline{\Pi}_{\mu\mu}^{-1})^{-1}\underline{\Pi}_{\mu\nu}^{-1}(\Delta-\underline{\Pi}_{\nu\nu}^{-1})^{-1}\underline{\Pi}_{\nu 1}^{-1}\vec{C}_1+...,$$

where Δ is a true eigenvalue of the total matrix and C_1 is a projection of the total eigenvector on the subspace. The elements of $\underline{\Pi}^{-1}$ could be arranged in order of importance with respect to $\underline{\Pi}_{11}^{-1}$ so that, for example, $\underline{\Pi}_{12}^{-1}$ is larger than $\underline{\Pi}_{13}^{-1}$ and so on. In practice, the series in Eq. (22) is rapidly convergent; and if one uses some of the optimization procedures outlined above, the first term on the RHS of Eq. (14) is all that is necessary for good results. Note that if we transform $\underline{\Pi}^{-1}(\omega)$ as we did in Fig. 1b, $(\Delta-\underline{\Pi}_{\mu\mu}^{-1})^{-1}$ is just the inverse of a diagonal matrix.

$$\underline{\Pi}^{-1}\vec{C} = \begin{pmatrix} \underline{\Pi}_{12}^{-1} & \underline{\Pi}_{12}^{-1} & \cdots & \\ \underline{\Pi}_{21}^{-1} & \underline{\Pi}_{22}^{-1} & & \\ \vdots & & \ddots & \\ \underline{\Pi}_{N1}^{-1} & \cdots & & \underline{\Pi}_{NN}^{-1} \end{pmatrix} \begin{pmatrix} \vec{C}_N \\ \vdots \\ \vec{C}_N \end{pmatrix}$$

Figure 2. Block Form for PH Propagator Matrix.

C. Investigation of Transition Metal Oxides.

1. Optical Properties - These investigations center especially on the properties of TiO. Our calculations and analyses of experiments, indicate that the optical reflectivities of titanium surfaces undergo significant changes as oxides are formed. These calculations identify previously unidentified peaks in the oxide spectra at about 8-10 eV and 26 eV as transitions from oxygen 2p and 2s bands, respectively. Our calculations also identify structures in the 5-6 eV region as involving d-bands. The d-band structure changes quite a lot under varying conditions of oxidation and can be used as an indicator of the oxide structure.

Our analysis indicates that the oxide produced initially by oxygen bombardment of the clean polycrystalline surface is TiO-like[5] with further banbardment producing a trend toward greater oxidation or perhaps a mixed oxide state but that the air exposed initial surface seems to be TiO_2. Oxygen exposure of the clean surface at room temperature produces a TiO structure which evolves at a much slower rate than for the single crystal.[6] The changes in the reflectivity data which accompany these different conditions of oxygen exposure are consistent with the assumed oxide structures. For example, in Fig. 3 we show the changes in the reflectivity which accompany continued oxygen bombardment. The structure around 5 eV, identified by our calculations as involving d-bands, reduces dramatically which is consistent with a trend toward TiO_2, in which case the valence d-bands would be completely depleted. Undoubtedly the condition of oxygen bombardment in these measurements prevents the surface from stabilizing. Certainly the differences among the oxides would be quite important in the mechanisms of oxide growth under various conditions, and these changes may well be useful in understanding the corrosion and possivation of metallic surfaces.

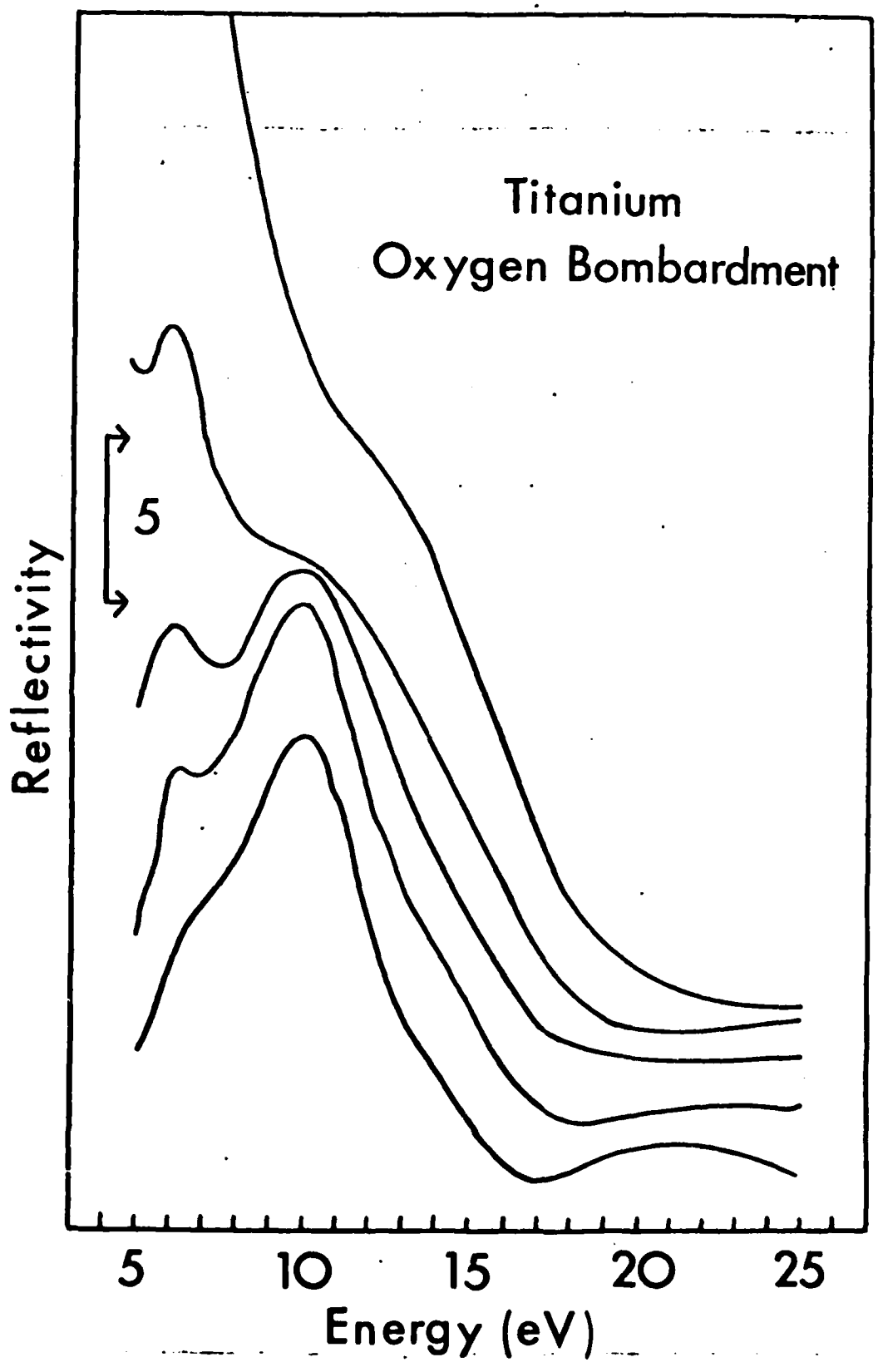

Fig. 3 Reflectivity after successive oxygen bombardments.

Let us look in more detail at the analysis of the TiO optical properties. The major components in the optical absorption spectra of all the oxides are several structures due to a d-band excitations at lower energies, a broader structure due mostly to O-2p band excitations (perhaps with some admixed d character) at intermediate energies, and a structure due to O-2s excitations at higher energies. All these interband structures are superimposed on a temperature-dependent intraband background which has a Drude-like frequency dependence of ω^{-3} at lower frequencies. The positions and strengths of the interband peaks vary with varying oxide structure so that the optical data provides a means for identifying the oxide. As an example of the optical behavior, we present the reflectance spectra[5] of various Ti surfaces in Fig. 4. The lower two curves are for oxide structures formed under different conditions. These curves show peak structures from about 5 to 6 eV to lower energies for which d-band transitions are assigned (actually, recent low temperature measurements show the d-band structure extends down to .2 eV. [7]). Transitions from the O-2p band region are assigned to the broad structure around 10 eV, which makes sense since this structure disappears for the clean surface. The assignment for the structure seen above 20 eV which peaks somewhere around 25 eV is O-2s, although transitions from the valence bands to higher conduction bands are also present.

To investigate this optical behavior, we need to look at the imaginary part of the macroscopic dielectric function

$$\varepsilon(\omega) = \lim_{\vec{q}\to 0} \varepsilon(\vec{q},\vec{q};\omega) \tag{15}$$

$\mathrm{Im}(\varepsilon(\omega))$ may be written[8]

$$\mathrm{Im}(\varepsilon(\omega)) \sim \frac{1}{\omega^2} \sum_{s,s'} F_s^{\alpha}\, \mathrm{Im}\,\Pi_{ss'}(\omega)\, F_{s'}^{\alpha *} \tag{16}$$

$$F_s^{\alpha} = \langle \psi_{ai} | \nabla_{\alpha} | \phi_{oj} \rangle$$

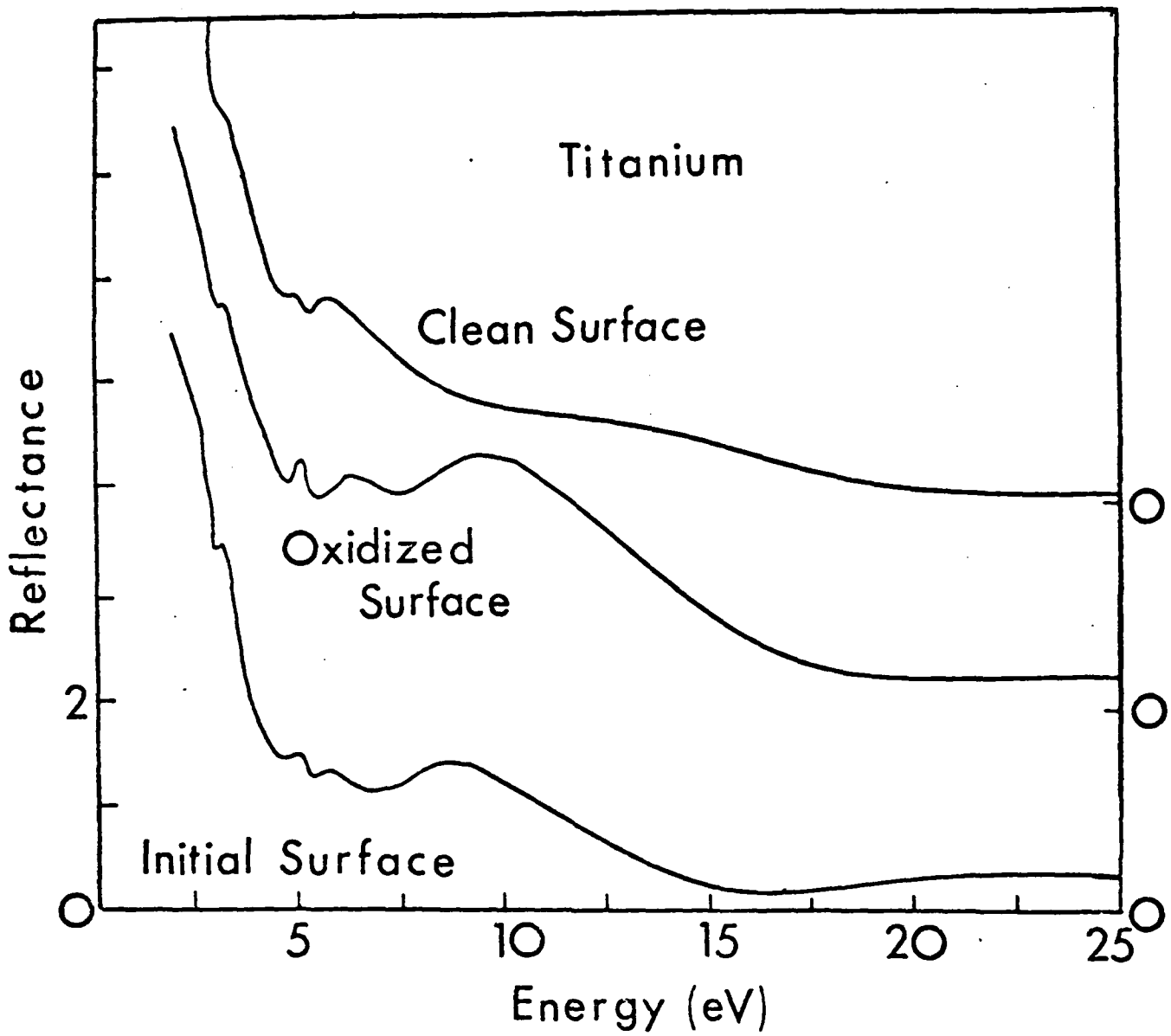

Fig. 4 Reflectance of clean and oxidized Ti surfaces.

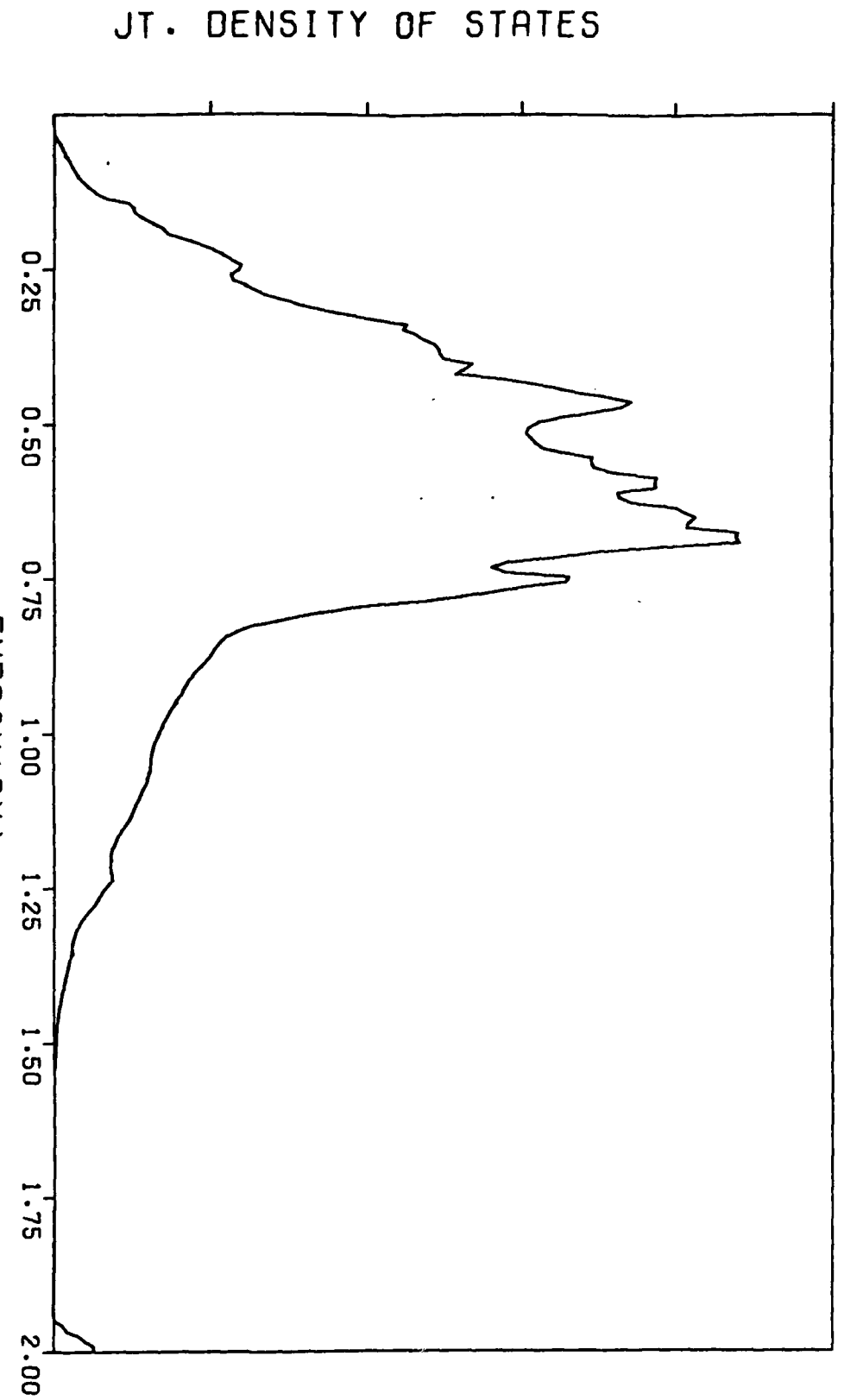

Fig. 5 Calculated joint density of states.

where the reducible polarization matrix $\underline{\Pi}$ has the structure given in Eq. (5). One may neglect the effect of the matrix elements F_s^α in Eq. (16) and the particle-hole interactions contained in $\underline{\Pi}$. Under these approximations, the macroscopic dielectric function is proportional just to the joint density of states.

To evaluate the importance of different effects on the optical behavior, we present in Fig. 5 the joint density of states calculated by us using uncorrelated HF energy bands.[9] For comparison we present in Fig. 6 the experimental joint density of states obtained from the Kramers-Kronig analyzed optical constants via the relation

$$N_J(\omega)_{exp} = \omega^2 \, \varepsilon_2(\omega)_{exp} \tag{17}$$

where

$$\varepsilon(\omega) = \varepsilon_1(\omega) - i\varepsilon_2(\omega)$$

We see that there is general agreement among the positions of the peak structures in the two spectra as indicated in Table 1. In order to identify the symmetry of the transitions involved we may consider the function

$$n_i(\omega) = \sum_{b,\vec{k}} |c_{b,v}i(\vec{k})|^2 \, \delta(\omega - E_b(\vec{k})) \tag{18}$$

where $c_{b,i}(\vec{k})$ is the Bloch coefficient for local orbital i in band b. Thus $n_i(\omega)$ is a measure of the density of states for a given local orbital. It turns out that orbitals of the same symmetry have local densities of states which are quite similar in the valence and conduction band regions so that we may plot representative O-2p and Ti-3d orbitals in Fig. 7. Actually, the orbital densities of states plotted are

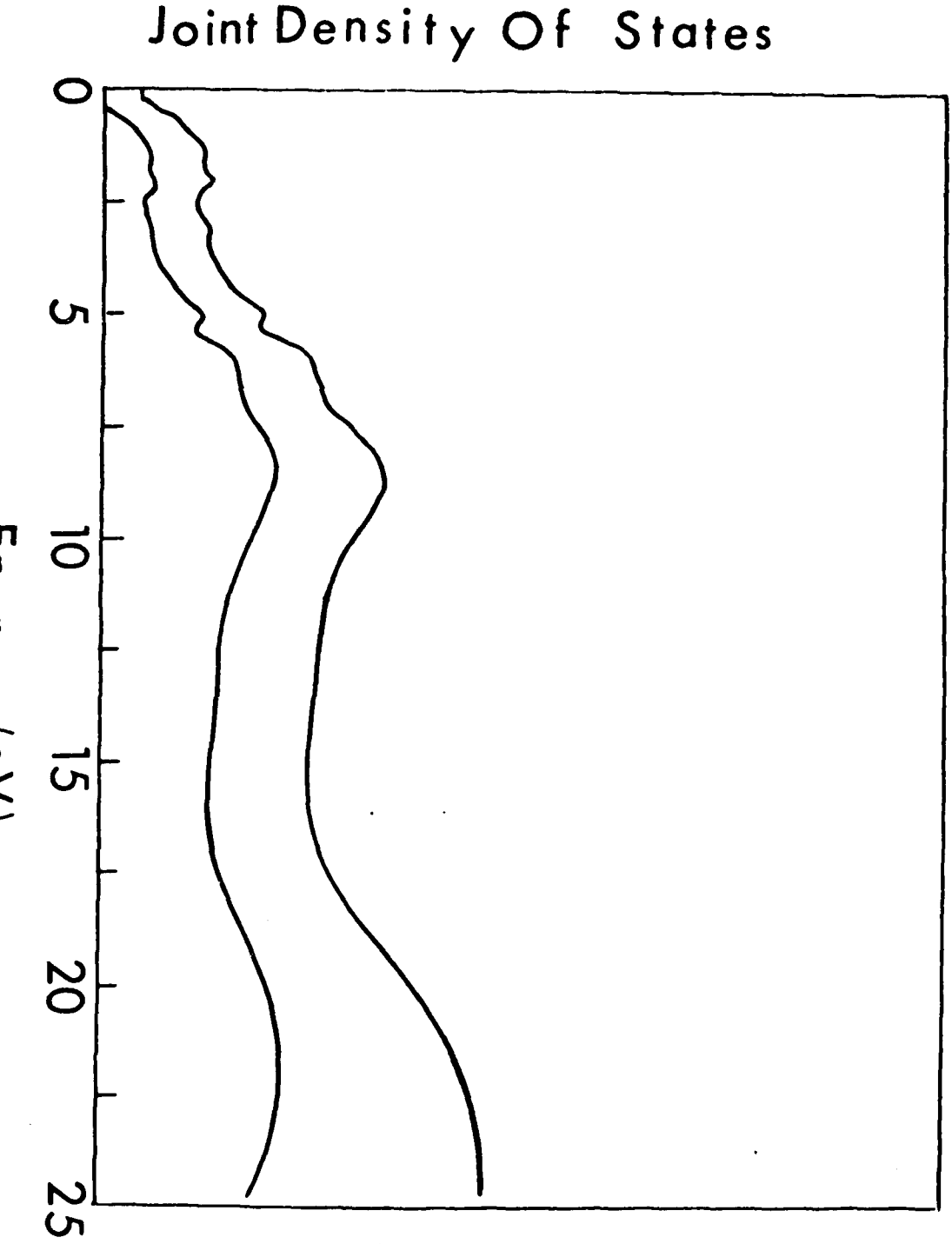

Fig. 6 Experimental joint density of states.

Table I. Comparison of peak maxima from the calculated and experimentally derived joint densities of states and Lynch's ε_2 data. All energies are in eV.

Calculated[a]	Experiment[b]	Lynch et. al[c]
3.28	3.32	3.2
5.44	5.20	5.6
6.34	6.45(shoulder)	
9.40 (central maximum)	8.78	8.2
31.	24.5	23.8

a. See Figure 5

b. See Figure 6

c. Ref. 9

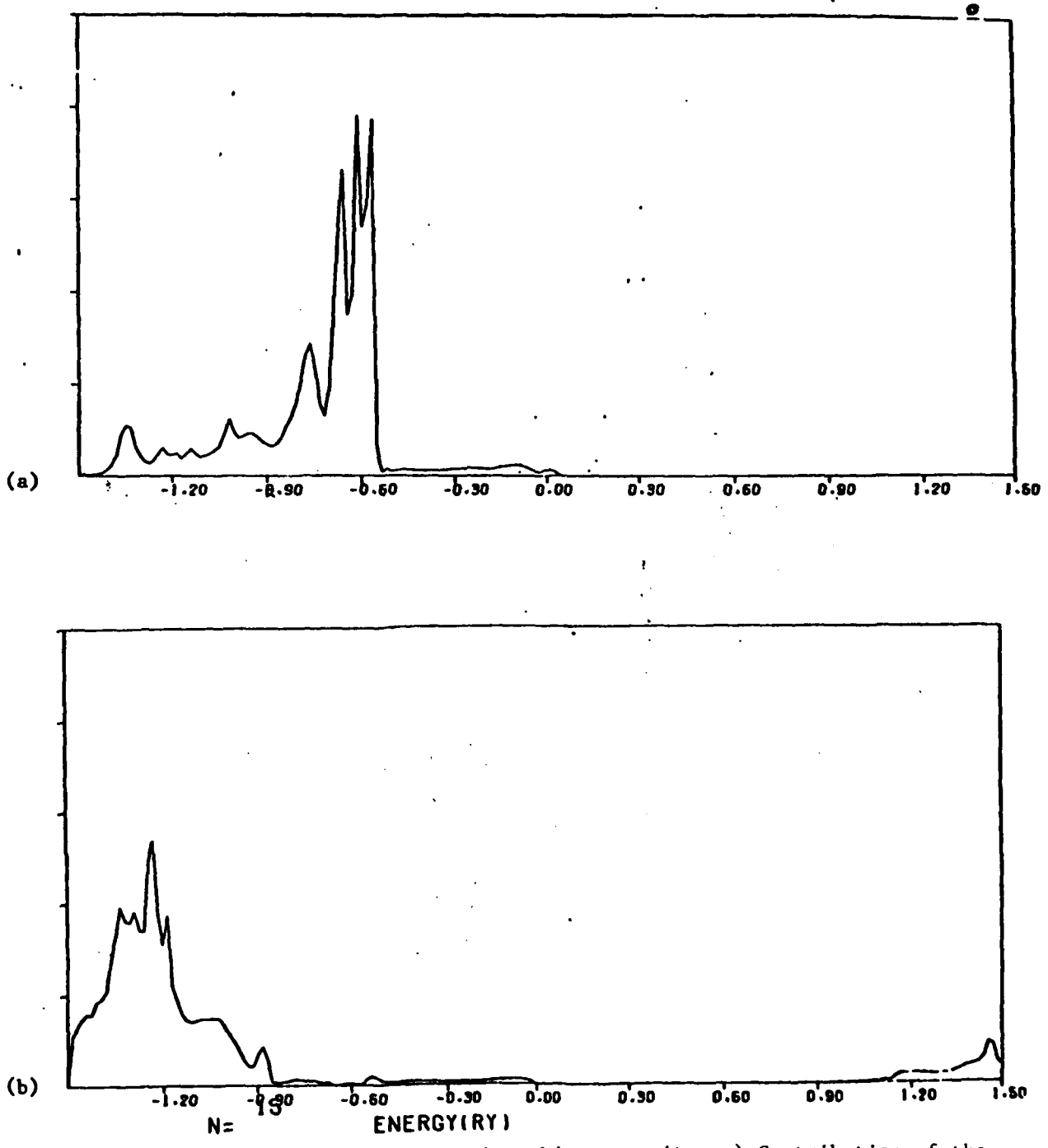

Fig. 7 Local densities of states in arbitrary units. a) Contribution of the the Ti-3d local orbital in the valence and conduction band regions. b) Contribution of the O-2p local orbital.

quite a bit larger than any of the others in the valence band region and are also about the same size as each other, the differences in Fig. 7 being attributable to different scalings. Thus the data in Fig. 7 supports assignments of p and d band regions in the optical spectrum, and results not shown here support our assignment of the peak at about 25 eV to O-2s transitions. Note that $n_d(\omega)$ in Fig. 7 is most prominent above the Fermi energy at -.888 eV, but that there is some mixing between the p and d states in the region just below the Fermi level. Whether this mixing actually occurs in the real system will be discussed below.

The first effect we may consider to improve our calculation is to include the matrix elements F_s^α in Eq. (16). These matrix elements have the effect of optical selection rules since they only connect states with angular momentum difference $\Delta\ell=\pm 1$. This effect can be quite significant for transitions between bands each of a particular symmetry, but the effect would be negligible for transitions between well-mixed bands. To see what is the case for TiO, we have recalculated the optical absorption with the matrix elements F_s^α included and have presented the results in Fig. 8. The shape is nearly the same as in Fig. 5, indicating the symmetry admixing depicted in Fig. 7, although there is a slight reduction of the structure at lower energy because the selection rule forbids d-to-d transitions, which are stronger in this region. Relaxation and correlation effects, discussed below, will separate the p and d-bands so that the lower energy structure will be further diminished.

2. Relaxation and Correlation Effects. To go beyond the HF approximation for the ground state properties of the system, it is necessary to consider self energy corrections. These corrections introduce relaxation and correlation effects to the single electron ionizations described by the energy band structure. The eigenvalue equation may be written

$$\left[\underline{H}_o + \underline{\Sigma}\ (\omega)\right]\ \vec{A}(\omega) = E(\omega)\ \vec{A}(\omega) \qquad (19)$$

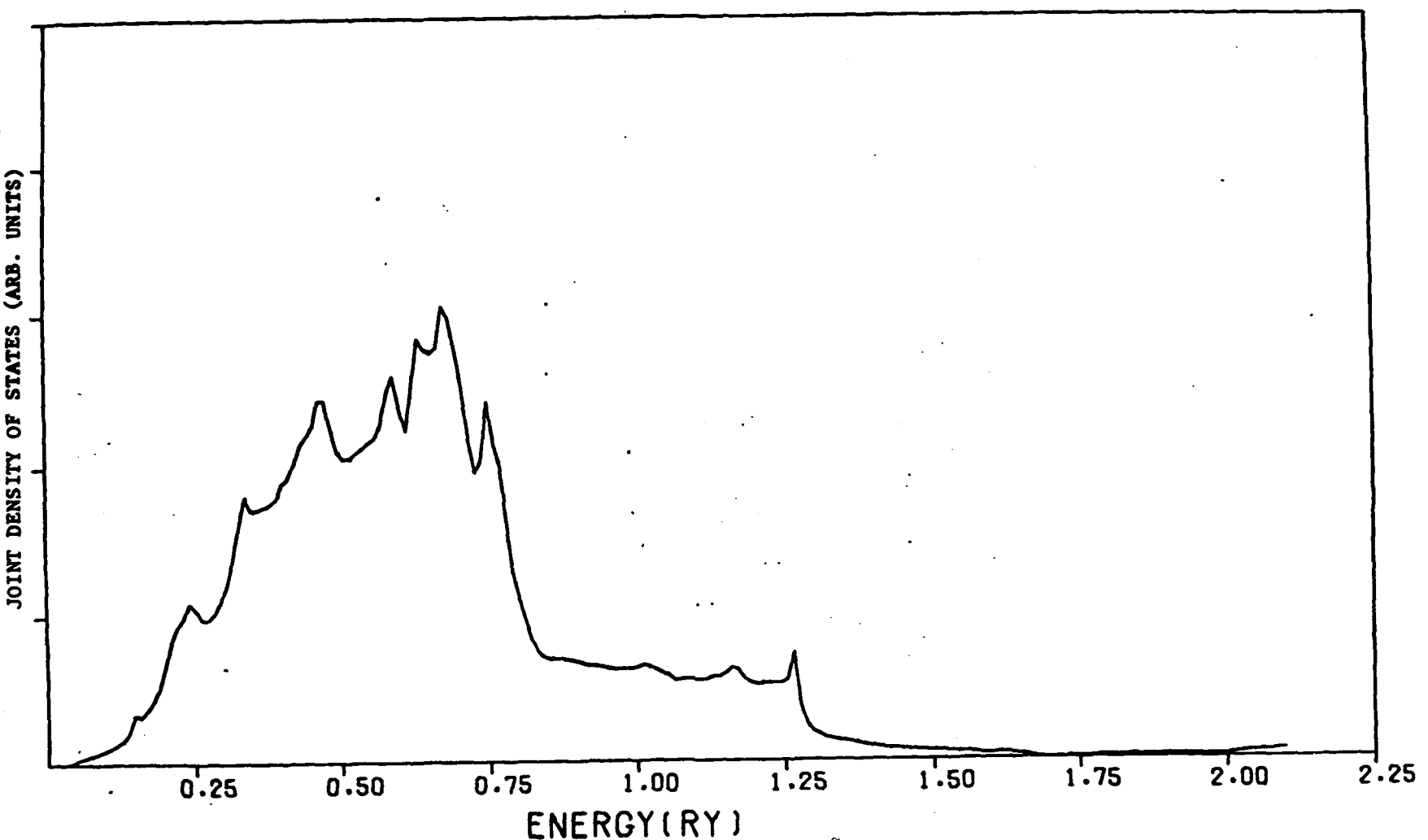

Fig. 8 Calculated joint density of states with matrix elements F_s^{α} included.

where H_o is the HF Hamiltonian, $\underline{\Sigma}$ is the self-energy, and E is our correlated band energy. Neglecting possible spin polarization effects, we may write the most important term in $\underline{\Sigma}$ as a dynamically screened exchange[10]

$$\Sigma^1_{k,k'}(\omega) = \frac{i}{2\pi} b^*_{\vec{k}i} b_{\vec{k}j} V_{i\ell,mn} V_{m'n',\ell j} \times \int \Pi_{mn,m'n'}(\vec{q},\omega') G^o_{k\ell,k'\ell'}(\vec{q},\omega+\omega') e^{i\delta\omega'} d\omega' \quad (20)$$

where k=kn, k'=kn' (The reduced momenta are the same). To avoid even more complicated notation, repeated indices in the equations for $\underline{\Sigma}$ indicate that the terms are to be summed over that index. In Eq. (20) $b_{\vec{k}j} \equiv a_{\vec{k}j} e^{i\vec{k}\cdot\vec{k}j}$ (no sum) where $a_{\vec{k}j}$ is the Bloch coefficient for state $\vec{k}$. $\underline{G}^o$ is the one-particle Green's function constructed with HF energy bands, and $\underline{\Pi}$ is given in Eq. (5) (Except that now it has an explicit q dependence). One can easily carry out the ω' integration; the result contains contributions from the poles of Π and from the poles of $\underline{G}^o$.[10]

A difficulty with Eq. (20) is that, unlike the optical absorption calculation where only $\vec{q}\to o$ is needed, one must find $\underline{\Pi}(\vec{q},\omega)$ for a sampling of $\vec{q}$ throughout the Brillouin zone. In our model this requires a repeated series of diagonalizations of large matrices. An alternative which retains some of the major effects we seek but is computationally much simpler is to use the second order expression for $\underline{\Sigma}^{sc}$. We would then replace $\underline{\Pi}$ by $\underline{\Pi}_o$ in Eq. (6). One can show that such an approximation neglects effects due to multiple particle-hole excitations or collective modes such as plasmons, but studies on highly inhomogeneous atomic systems[10] for which the electron-electron interactions should be strong indicate the correct relative sizes for relaxation and correlation contributions are given by the second-order calculation. For solid state systems, where collective modes are more significant, the second-order calculations would not describe regions of the photoemission spectrum, for example, where plasmons dominate. However, one can immediately write down the expression for $\underline{\Pi}^o$ without doing any diagonalizations or inversions, and the two-electron integral sums are similar to the ones we did for the optical absorption case.

The first step in the calculation is to transform Eq. (19) to the basis of HF Bloch states. Then we have

$$E_o \underline{I} + \underline{\Sigma}(\omega) \quad \vec{A}(\omega) = E(\omega) \vec{A}(\omega), \tag{21}$$

where $\underline{I}$ is the identity matrix. The effect of Eq. (21) is to admix the HF band states. But ω appears in the equation as a parameter, and a complete solution for the band structure could be written schematically as

$$E = E_o + \Sigma(E).$$

Therefore we want solutions of Eq. (21) for values of ω near the band energies of interest. In practice we solve Eq. (21) for a sampling of frequencies in the energy range (e.g., the valence band region) we are studying.

We have applied the above method to calculating relaxation and correlation corrections[11] to the HF energy bands of Jennison and Kunz.[9] Originally these bands were thought to be in agreement with XPS measurements[12] of the O-2p, Ti-3d valence band density of states for TiO, but subsequent measurements[13] showed the first experiments to be in error. Our calculations show that the self-energy correction makes the O-2p and Ti-3d bands move away from one another with an accompanying reduction of s,d admixing, in agreement with the latest experiments. This agreement is gratifying since this method makes the important effect of d-band intrasite correlations and the formation of Hubbard bands accessible to calculations.

IV. REFERENCES

1. A. B. Kunz, Phys. Stat. Sol. 36, 301 (1969).
2. A. L. Fetter and J. D. Walecka, Quantum Theory of Many Particle Systems, (McGraw-Hill, New York, 1971).
3. H. Ehrenreich and M. H. Cohen, Phys. Rev. 115, 786 (1959).
4. W. Hanke and L. J. Sham, Phys. Rev. B12, 4501 (1975).
5. W. Wall, M. W. Ribarsky, and J. R. Stevenson, J. App. Phys., to be published.
6. H. D. Shih and F. Jona, App. Phys. 12, 311 (1977).
7. D. W. Lynch, C. D. Olson, and J. H. Weaver, Phys. Rev. B 11, 3617 (1975).
8. M. W. Ribarsky, Bull. Am. Phys. Soc. 22, 550 (1977).
9. D. R. Jennison and A. B. Kunz, Phys. Rev. Lett. 39, 418 (1977).
10. M. W. Ribarsky, Phys. Rev. A 12, 1739 (1975).
11. M. W. Ribarsky, in preparation.
12. K. I. Ichikawa, O. Terasaki, and T. Sagawa, J. Phys. Soc. Jpn. 36, 706 (1974).
13. V. E. Henrich, H. J. Zeiger, and T. B. Reed, Phys. Rev. B 17, 4121 (1978).

V. COMMUNICATIONS

The following communications have taken place or they are being planned as a result of this research.

A. Papers Presented

"Excitation Structure of TiO", M. W. Ribarsky. Bull. Am. Phys. Loc. 22, 550 (1977).

"Calculations of the Optical and X-Ray Emission Spectra of TiO", M. W. Ribarsky, Bull. Am. Phys. Soc. 24, 392 (1977).

B. Papers Accepted for Publication

"Optical Properties of Titanium and Titanium Oxide Surfaces", William E. Wall, M. W. Ribarsky, and J. R. Stevenson, to be published, J. App. Phys. (Jan., 1980).

C. Papers in Preparation

"Excitation Structure and Optical Properties of TiO," M. W. Ribarsky, to be submitted.

"Electron Correlation in TiO and its Effect on the Band Structure, M. W. Ribarsky, in preparation.

D. Research Group Interactions.

1. D. R. Jennison, Sandia Laboratories, Albuquergue, New Mexico.
2. A. B. Kunz, Physics Dept, University of Illinois - Urbana.
3. P. J. Feibelman, Sandia Laboratories, Albuquerque New Mexico.
4. Frank Tobin, Chemistry Dept., The Johns Hopkins University.

VI. PERSONNEL

The following individuals have participated in the research described above.

1.	Dr. M. W. Ribarsky	Principal Investigator
2.	William D. Luedtke	Graduate Student

In addition to the above personnel, this research has benefitted from interactions with experimental research group at Georgia Tech. Among the members who have helped are Dr. Keith Legg, Research Scientist, and Dr. James R. Stevenson, Professor.

VII. APPENDIX

The following paper was supported in part by this grant and will appear in the January, 1980 issue of the Journal of Applied Physics.

Submitted for publication in
J. Appl. Phys.

Optical Properties of Titanium and Titanium Oxide Surfaces*

by

William E. Wall, M. W. Ribarsky, and J. R. Stevenson

Georgia Institute of Technology, Atlanta, Georgia 30332 U.S.A.

The near normal incidence reflectivity of titanium has been measured for photon energies of 2 eV to 25 eV under closely controlled surface conditions. Measurements, using synchrotron radiation above 5 eV, were made in ultra high vacuum on both clean and in-situ oxidized surfaces monitored with Auger spectroscopy. The reflectivity data were Kramers-Kronig analyzed to generate the optical constants. Structure in ε_2 appearing in the oxidized surface but absent in the clean surface is related to the oxygen 2p and 2s bands. Some differences in the oxide structure are observed between oxide films grown on titanium exposure to oxygen compared to exposure to an oxygen plasma.

---

*Supported in part by AFOSR under grants 75-2773 and 76-3108.

INTRODUCTION

The optical properties of titanium and its oxides have not been extensively reported in the literature even though titanium is a widely used industrial material with many physical and chemical properties of interest in materials applications. The oxide phases have a variety of structures and electrical properties which range from metallic behavior in TiO to insulating behavior in TiO_2. Suggestions have been made that these phase changes accompany oxide growth and that the onset of passivation in the oxide films may even be related to changes in phase.[1] Most of the optical studies attempted have been on metallic titanium,[2,3] although the present work indicates that a residual oxide was present in these previous studies. A systematic study of oxide growth on titanium has not been reported in which the growth of the oxide was monitored with optical measurements.

In this paper we report measurements of the optical properties of oxides of various thicknesses grown on titanium under a variety of conditions. The optical properties were derived from reflectance data taken in the range 2 to 25 eV with some data extended to 40 eV. The data were Kramers-Kronig analyzed and the values for ε_1 and ε_2 obtained. Auger spectra were taken on the same surfaces as the reflectance measurements, allowing us to monitor the surface cleanliness. The analysis of the Auger lineshapes was critical in indicating the possible oxide structures formed. An analysis based on the reflectivity data alone would have been insufficient to identify the oxide structures.

In this paper we compare the results of our reflectivity measurements with the results of other measurements, and note the differences among the spectra. Identification of the structure in the oxide optical constants with

transitions between the oxide valence and conduction bands is made by comparing with band structure calculations.[4] Analysis of our Auger spectra also indicates that the final oxide structure for our oxygen exposed polycrystalline Ti surface but not our oxygen bombarded surface is similar to the final structure observed by Shih and Jona[5] for an oxygen exposed single crystal surface.

EXPERIMENTAL

Near normal incidence optical reflectivity and Auger spectroscopy measurements were performed on polycrystalline titanium samples. All of the measurements were made in an ultra high vacuum system with a base pressure of $<1\times10^{-10}$ Torr. Radiation from the University of Wisconsin Synchrotron Radiation Center was used as the light source for photon energies greater than 5 eV with conventional tungsten and discharge lamps used for the low energy end of the spectrum. The sample chamber, illustrated in Figure 1, is designed such that optical reflectivity and Auger measurements can be made without repositioning of the sample, allowing near simultaneous measurements. A sputter ion gun and a sample heater are included in the chamber for surface cleaning and oxidation studies. A quadrupole residual gas analyser and high purity gas manifold are also attached to the system. Figure 2 shows schematically the instrumentation configuration. Both optical and Auger measurements are performed automatically by a computer based data acquisition system described elsewhere.[6]

Samples 12.7 mm diameter and 2 mm thick were cut from commercially prepared electron beam zone refined titanium rod having a nominal purity of 99.97%. Major impurities included oxygen ($\sim$150 ppm) and Carbon ($\sim$50 ppm). The samples were mechanically polished with a final polish of .05 micron alumina. Following the mechanical polish, the samples were placed in a trichloroethylene vapor degreaser for five minutes, washed in acetone, and etched for approximately 5 seconds in a solution of HF, H_2O_2, and H_2O. Following the etch the sample was washed in distilled water and blown dry.

The sample was immediately mounted and placed in the vacuum chamber,

pumped down, and the whole system baked at 200°C for ∿24 hours. At this point the Auger spectra show strong carbon and oxygen lines, while the titanium line is distorted by the superposition of a nitrogen Auger line.[7] Heating the sample to 700°C for 24 hours removed these impurities; however large Auger peaks of sulfur and chlorine appeared, presumably segregating on the surface from the bulk.[8] A short period of Ar sputtering (30 seconds, 10μA/cm^2 at 3 keV) while the sample was being heated removed these contaminants, leaving the surface clean to the limits of detection (approximately 1% atomic). LEED studies performed on titanium after similar cleaning procedures showed an ordered surface.[9] The optical and Auger spectra, after sample cooling, would remain stable for ∿1 hour in the ∿1x10^{-10} Torr vacuum. A short heating period of 30 minutes to 600°C followed by a 30 second Ar sputtering at 600°C was sufficient to reclean the sample. All reflectivity measurements on the clean sample were made during the 1 hour "clean period".

A series of optical and Auger measurements after exposure to controlled amounts of oxygen were made. The oxygen exposure varied from 5 Langmuir (1 Langmuir = 10^{-6} Torr - sec) to 10,000 L, all at room temperature. Subsequently, measurements were made on the sample after a series of oxygen ion bombardments (energies of 1 keV and 2 keV). Finally, Ar sputtering and sample heating were used to reclean the sample in order to check the reproducibility of the clean surface data.

EXPERIMENTAL RESULTS

In the following measurements the initial surface spectrum is that of the sample when first placed in the sample chamber. Ellipsometric measurements o

Ti under similar conditions indicate a TiO_2 surface layer of about 85 Å thickness.[8] The clean surface spectra were measured following the cleaning procedure previously described. The oxidized surface spectra occurred after bombarding the sample with 1 keV oxygen ions at 15μA/cm^2 for 7.5 minutes.

In Figure 3 we compare the reflectance spectra for the titanium surfaces. We attribute the structures below 7 eV to transitions within the d-band region although there is undoubtedly some s and p mixing in these bands. This interpretation is consistent with that of Lynch et al.[10] and also with Ti $L_{II,III}$ x-ray emission and absorption data[11] which give an indication of the shapes and relative energy positions of the valence and conduction bands, respectively. We attribute the peak around 10 eV and the structure beyond 20 eV in the oxidized and initial surface spectrum to transition from the oxygen 2p and 2s bands, respectively, although the width of the latter structure indicates transition from the valence to higher bands may also be present. These peak assignments are consistent with energy band calculations[4] which indicate transitions involving the oxygen 2s and 2p bands should occur at these energies. In addition, the separation of 16 eV between the two peaks in the initial surface spectrum is just the free-atom value and has been seen in the XPS spectrum of TiO_2.[12] It is to be noted that these two peaks are at lower energy in the initial surface spectrum as compared to the oxide spectrum. We believe the spectra differ because a TiO-like phase exists on the oxidized surface whereas reduced TiO_2 exists on the initial surface. These oxides are not stoichiometric, and the air-exposed surface may even be hydrated. However, our viewpoint is corroborated by the Auger data which show an oxygen peak-to-peak height twice as large for the initial surface as for the oxidized surface, and also show lineshapes indicative of these oxide

phases. In addition, there is a reduction in the height of the d-band structure between 5-7 eV relative to the oxygen 2p band in the initial surface reflectance as compared to the oxidized surface. Reduced TiO_2 should have a much lower occupation in the d-band region than TiO. Recent UPS measurements of TiO exposed to oxygen[13] show that there is indeed a dramatic reduction of the d-band structure under oxygen exposure. In these results[13] the Fermi level also moves about 1 eV closer to the valence band as the sample is oxidized with a position at maximum oxygen exposure the same as for stoichiometric TiO_2. This movement is consistent with the change in position of the oxygen 2p band displayed in Figure 4.

For comparison we present the spectrum of Lynch et al.[10] and our cleanest surface spectrum in Figure 4. The peaks around 10 eV and 25 eV appearing in Lynch's data disappear in ours, although a shoulder at about 13 eV remains. The Lynch spectrum falls somewhere between our initial surface and oxidized surface spectra.

Figure 5 shows the reflectance spectra after successive oxygen bombardments with the build-up of the oxygen peak at about 10 eV, the movement to lower energy and build-up of the oxygen peak above 20 eV, and the reduction of the d-band structure between 5-7 eV. Note that although the bombardment builds an oxide much thicker than that on the initial surface, none of the spectra match the initial surface spectrum. In particular the peak at 10 eV remains fixed in energy even for the thick oxides, and does not move to lower energy as for the initial surface. However, the peak above 20 eV does not move to lower energy and the d-band structure is reduced, these features being comparable to the initial surface structure. It is possible that during the oxygen bombardment regions of different oxide structure are formed on the

surface. The predominant structure might be TiO-like, but with regions having TiO_2 structure. The reflectance spectrum would then show a combination of the features of these oxides. The fact that a sub-stoichiometric oxide may continue to grow under oxygen bombardment to a thickness much greater than the initial surface thickness indicates different conditions of exposure can produce quite different oxide structures. This result may be of consequence in the study of the mechanisms of oxide growth and in the search for means to control oxide growth rates.

We must analyze the Auger lineshapes in detail to obtain further information about the surface oxide structure. Our Auger spectrometer has an energy resolution $\Delta E/E$ of about .6% so that these measurements in the range from 300 to 500 eV have a resolution of 2 to 3 eV. The Auger spectra in Fig. 6 are for the surface depicted in the reflectance spectra of Fig. 3. The figure shows the Ti $L_{II,III}$ and O KLL structure. The clean surface Ti $L_{II,III}$ spectrum is identical to those of Solomon and Baun[14] for a freshly evaporated film and Shih and Jona[5] for the Ti(001) surface. The initial surface and oxidized surface spectra have peak to peak ratios between the dominant Ti LMM structure and the O KLL structure which when adjusted for transition probabilities are 2:1 and 1:1, respectively. This result suggests a TiO_2 structure on the initial surface and a TiO structure on the oxidized surface. The initial surface spectrum is nearly the same as the TiO_2[14] Auger spectrum shown in Fig. 4 of Ref. 14 except that the shoulder at about 420 eV is more pronounced in our spectrum. The most prominent difference between our oxidized surface spectrum and the TiO spectrum in Fig. 4 of Ref. 14 is the absence in our spectrum of the shoulder feature at about 410 eV in the Ti LMM structure.

We studied the effects of oxidation under different conditions on the

Auger spectra. The above oxygen bombarded surface corresponds to about 500 L oxygen exposure. At about 100 L exposure to oxygen gas at room temperature, the Auger spectrum of Shih and Jona[5] for Ti(001) was already identical to the TiO spectrum. Further oxygen bombardment for several more minutes produced the changes in the reflectivity noted in Fig. 5, but the Auger spectrum did not change much and in particular the Ti/O peak ratio remained the same.

We also studied the effects of oxidation at room temperature on our polycrystalline Ti sample . In this case the pattern of change in the Ti $L_{II,III}$ spectrum observed by Shih and Jona[5] was also observed by us, but the changes were much slower with respect to oxygen exposure. Shown in Fig. 7 are the spectra at 500 L and 10^4 L oxygen exposure. At 500 L one can clearly see the feature at 410 eV, but it is still less pronounced than in the Shih and Jona spectrum at 100 L. After 10^4 L exposure, our spectrum is identical with that of Shih and Jona and also with the TiO spectrum[14]. At 500 L the reflectance spectrum is nearly the same as our oxidized surface spectrum in Fig. 3; and, unlike the oxygen bombarded case, the reflectance remains about the same for greater oxygen exposures.

KRAMERS KRONIG ANALYSIS

A Kramers-Kronig analysis was used to derive the phase θ of the complex reflectance $re^{i\theta}$ from the reflectivity data and thus to derive the complex refractive index and the complex dielectric function. For energies below 2 eV, the same reflectance data segment, taken from measurements by Lynch *et al.*,[10] was used throughout. As we discuss below, this low energy approximation did not affect the location of structure in optical constants derived from the KK analysis in the region of 2-25 eV.

Since an infinite integral of the reflectivity over frequency is necessary to obtain the phase information, a high energy extrapolation of the data was needed. We used a standard power law extrapolation of the form $R(E) = R_o E^{-\beta}$ for the reflectivity. Such extrapolations are usually not accurate because of high energy structure present in most materials, unless the exponent β can be fitted to give a known quantity, such as an independently obtained optical constant, at a given energy.[10] However, we have been able to obtain consistent results using a method which requires no independently obtained optical parameters. We fit the parameter β such that one of the sum rules[15]

$$\int_0^\infty (n-1)d\omega = 0 \qquad (1)$$

or

$$\int_0^\infty (n-1)\ \omega d\omega = 0 \qquad (2)$$

is satisfied. The latter constraint, Eq. (2), depends less on high frequency structure than does the former[16], and thus we use Eq. (2) to fit the extrapolated curve. For the data considered here, Eq. (1) also has a reasonably small value in all cases.

The various segments of the reflectivity spectrum from the discharge source and from the synchrotron had to be scaled to provide a smooth curve. In order to test the effect on the optical constants of this scaling and of the extrapolation procedure used, we calculated the optical constants of the oxidized titanium surface for two extreme cases of scaling. In both cases the parameter β was fit to satisfy Eq. (2). Figure 8 compares the joint density

of states for these two scalings. It is seen that the spectral shapes compare well up to about 18 eV with peak shifts of no more than a few percent, but that the final peak at 22-25 eV shifts by 3-4 eV, as is to be expected since this peak is at the edge of the data. Since the shapes of our reflectivity spectra are given much more accurately than their magnitudes, the positions and relative magnitudes of the peaks in the optical constants are reliable, with some shifting possible for the structure above 20 eV. Note that in Figure 8 the scaling has not affected the spectral shape below 2 eV.

ANALYSIS OF OPTICAL CONSTANTS

The complex refractive index n-ik, derived from our reflectances and phase results, can be used to construct the complex dielectric function via the expression

$$\varepsilon_1 - i\varepsilon_2 = (n-ik)^2$$

The quantity ε_2 gives the absorption spectrum of the system and therefore describes the excitation structure. If one neglects final state effects introduced by the interaction of the excited electron with its hole and also neglects any intraband contributions so that only direct, interband transitions contribute, then $\varepsilon_2(\omega)$ has the form

$$\varepsilon_2(\omega) \sim \frac{1}{\omega^2} \sum_{n,s} \sum_{BZ} \delta(\omega_{n,s}(\vec{k})-\omega) \left|M_{n,s}(\vec{k})\right|^2 d^3k \qquad (3)$$

The subscripts n and s refer to filled and unfilled bands respectively, and $\omega_{n,s}(\vec{k}) = \omega_n(\vec{k}) - \omega_s(\vec{k})$. The momentum matrix element $M_{n,s}(\vec{k})$ between states in bands n and s is nearly constant for bands with little dispersion. Then

$$\varepsilon_2(\omega) \sim \frac{1}{\omega^2} \; N_J(\omega) \qquad (4)$$

where $N_J(\omega)$ is the joint density of states.

The KK analyzed spectra of ε_1 and ε_2 for the clean, the oxidized, and the initial titanium surfaces are shown in Figure 9. The changes in structure among the ε_2 spectra are in most cases similar to the changes in the reflectivity spectra in Figure 4. Note, however, that the peak position at about 10 eV in the oxidized ε_2 spectrum is closer to the position in the initial spectrum than are the peak positions in the corresponding reflectivity spectra. The structure is also less pronounced in the ε_2 spectra than the corresponding structure in the reflectivity data.

To gain a more detailed understanding of the oxide structure, we may compare our results with the densities of states calculated by Schoen and Denker (SD).[4] These calculations take the defect character of the oxide into account, allowing for a 15% vacancy concentration and the non-stoichiometry of the oxide, and the valence bands are in substantial agreement with the most recent XPS measurements on TiO_{1+x}.[13] Though we do not have the joint densities of states from these calculations, we may note from Eqs. (3) and (4) above that structures in the density of states which are at different energies but are from the same regions in the Brillouin zone can be related to structure in the optical spectrum. Upon studying Fig. 1 in SD, showing the band structure and density of states for stoichiometric TiO with 15% vacancies, we see that indeed the prominent structures there can be linked to the structure in the joint density of states for the oxidized surface, the topmost curve in Fig. 8. The O-2p density of states will link strongly to the mostly d-like first peak in the conduction band, the peak regions in the two densities coming mostly from parallel bands in the Brillouin zone with the peaks separated by about 9 eV, in agreement with our assignment of the structure in Fig. 8. The O-2s band will have a weaker transition to the s-p

hybridized bands centered about 1.25Ryd in the density of states giving a separation of about 26 eV, again in agreement with experiment, although the breadth of the experimental structure may indicate transitions from the valence bands to higher conduction bands also contribute. The characteristic d-band double peak structure at about 5-6 eV in Fig. 8 may be due to transitions to the double-peaked hybridized s-p density of states in Fig. 7 of SD, or it may be due to structure in the valence d-band density of states itself, as indicated by the calculation of Ern and Switendick.[17] The results of SD for other compositions of TiO_{1+x} also support our assignments of transitions, although the transition energies would vary somewhat.

Comparison with the energy band calculations for TiO allows assignments of the peaks in the optical spectrum, but the calculations in themselves do not enable us to identify the oxide structure as TiO. Comparison with other band structures for different oxide compositions would probably allow similar assignments for the optical constants. However, the identification of the peaks in the 5-6 eV region of the oxidized spectrum as d-transitions and there subsequent decrease under further oxygen bombardment or air exposure indicates much further oxidation occurs in these cases. Still, the Auger lineshapes are necessary to make clear identifications of the oxide strucure.

CONCLUSIONS

The reflectivities of titanium surfaces undergo significant changes as oxides are formed. Careful cleaning monitored by Auger spectroscopy is necessary to insure a clean Ti surface, and several previous Ti reflectivity measurements show significant structure due to residual oxides. Cycles of oxygen bombardment followed by Argon sputtering yield reproducible

reflectivity spectra. The previously unidentified peaks at about 8-10 eV and 26 eV in the reflectivity spectra are most likely due to transition from oxygen 2p and 2s bands, respectively. Band structure calculations, x-ray emission and absorption data, and x-ray photoelectron data which show similar band separations for several other transition metal oxides support this conclusion.

The oxide produced initially by oxygen bombardment on the clean surface seems to be TiO-like with further bombardment producing a trend toward greater oxidation or perhaps a mixed oxide state, but the air exposed initial surface seems to be TiO_2. Oxygen exposure of the clean surface at room temperature eventually produces a stable TiO structure, but the structure evolves at much greater oxygen exposures than for the single crystal.[5]

The changes in the reflectivity data which accompany these different conditions of oxygen exposure are consistent with the assumed oxide structures, but the reflectivity in itself is not sufficient to identify the oxide structures. Comparisons of Auger peak heights and especially investigations of Auger lineshapes are necessary to identify oxide structures. On the other hand, certain trends in the reflectivity data, such as shown in Fig. 5, are not readily apparent in the Auger data. Both types of measurement were necessary in this work to identify important trends in the oxide growth.

Other investigators have seen changes in oxide structure under different conditions of exposure. Recent measurements by Garner *et al.*,[18] of the initial oxidation stages of the Si(111) surface indicate that different oxide structures form depending on whether the oxygen gas is excited or not. The SiO_2 structure occurs only for exposure to excited oxygen. Undoubtedly the condition of oxygen bombardment in our measurements prevents the surface from

stabilizing, and our air exposed oxide surface may have a more complicated structure, such as a hydrated structure which would be difficult to detect. Certainly the differences among these oxides may be quite important in the mechanisms of oxide growth under various conditions, and we are planning further investigations along these lines.

REFERENCES

1. J. O. M. Bockris, A. K. N. Reddy, and B. Rao, J. Electrochem. Soc. 113, 1132 (1966).

2. M. M. Kirillova and B. A. Charikov, Fig. Metal. Metaloved. 19, 495 (1965); I. D. Mash and G. P. Motulevich, Sov. Phys. - JETP 36, 516 (1973).

3. P. B. Johnson and R. W. Christy, Phys. Rev. B9, 5056 (1974); G. Hass and A. P. Bradford, J. Opt. Soc. Am. 47, 125 (1957).

4. J. M. Schoen and S. P. Denker, Phys. Rev. 184, 864 (1969).

5. H. D. Shih and F. Jona, App. Phys. 12, 311 (1977).

6. William E. Wall and James R. Stevenson, Nuclear Instruments and Methods, 152, 141 (1978).

7. H. D. Shih, K. O. Legg, and F. Jona, Surface Sci. 54, 355-364, (1976).

8. Tennyson Smith, J. Opt. Soc. Am. 62, 774 (1972); Tennyson Smith, Surf. Sci. 38, 292 (1973).

9. H. D. Shih, F. Jona, D. W. Jepsen, and P. M. Marcus, J. Phys. C: Solid State Phys. 9, 1405 (1976).

10. D. W. Lynch, C. G. Olson, and J. H. Weaver, Phys. Rev. B 11, 3617 (1975).

11. David W. Fischer, J. Appl. Phys. 41, 3561 (1970).

12. S. Hufner and G. K. Wertheim, Phys. Rev. B 8, 4857 (1973).

13. Victor E. Henrich, H. J. Zeigler, and T. B. Reed, Phys. Rev. B 17, 4121 (1978).

14. J. S. Solomon and W. L. Baun, Surf. Sci. 51, 22 (1975).

15. M. Altarelli, D. L. Dexter, H. M. Nussweig, and D. Y. Smith, Phys. Rev. B 6, 4502 (1972).

16. H. W. Ellis and J. R. Stevenson, J. Appl. Phys. 46, 3066 (1975).

17. V. E. Ern and A. C. Switendick, Phys. Rev. 137, A1927 (1965).

18. C. M. Garner, I. Lindau, C. Y. Su, and W. E. Spicer, BAPS 24, 277 (1979).

Figure Captions

Fig. 1. Cutaway view of ultrahigh vacuum chamber with apparatus for Auger and optical reflectivity measurements.

Fig. 2. Instrumentation configuration for the experimental chamber. The ellipsometer instrumentation shown is under development and was not used in this work.

Fig. 3. Reflectance spectra for various Ti surfaces.

Fig. 4. Comparison of our cleanest surface spectrum with the measurements of Lynch, Olson, and Weaver.[10]

Fig. 5. Reflectivity of Ti under oxygen bombardment. The top curve is the cleanest surface, and the curves below are after successive oxygen bombardments. Each set of data is offset for clarity with the bracket indicating a 5 percent change in reflectivity.

Fig. 6. Auger spectra taken just prior to the optical measurements. The positive excursion of the first major Ti core-core Auger line in the initial and oxidized surface spectra is due to a coincident nitrogen Auger line. Note that the ratio of the O to Ti peak-to-peak heights is twice as large in the initial surface spectrum as in the oxidized surface spectrum.

Fig. 7. Ti LMM Auger spectra at 500 L and 10^4L oxygen exposure. The latter spectrum is identical with that for TiO.[14]

Fig. 8. Joint density of states for the Kramers-Kronig analyzed reflectivity data using two extreme cases of scaling of the raw reflectivity data.

Fig. 9. Optical constants obtained from the Kramers-Kronig analysis of the reflectivity data. Each curve is offset as indicated. (a) The real part of the dielectric constant. (b) The imaginary part of the dielectric constant.

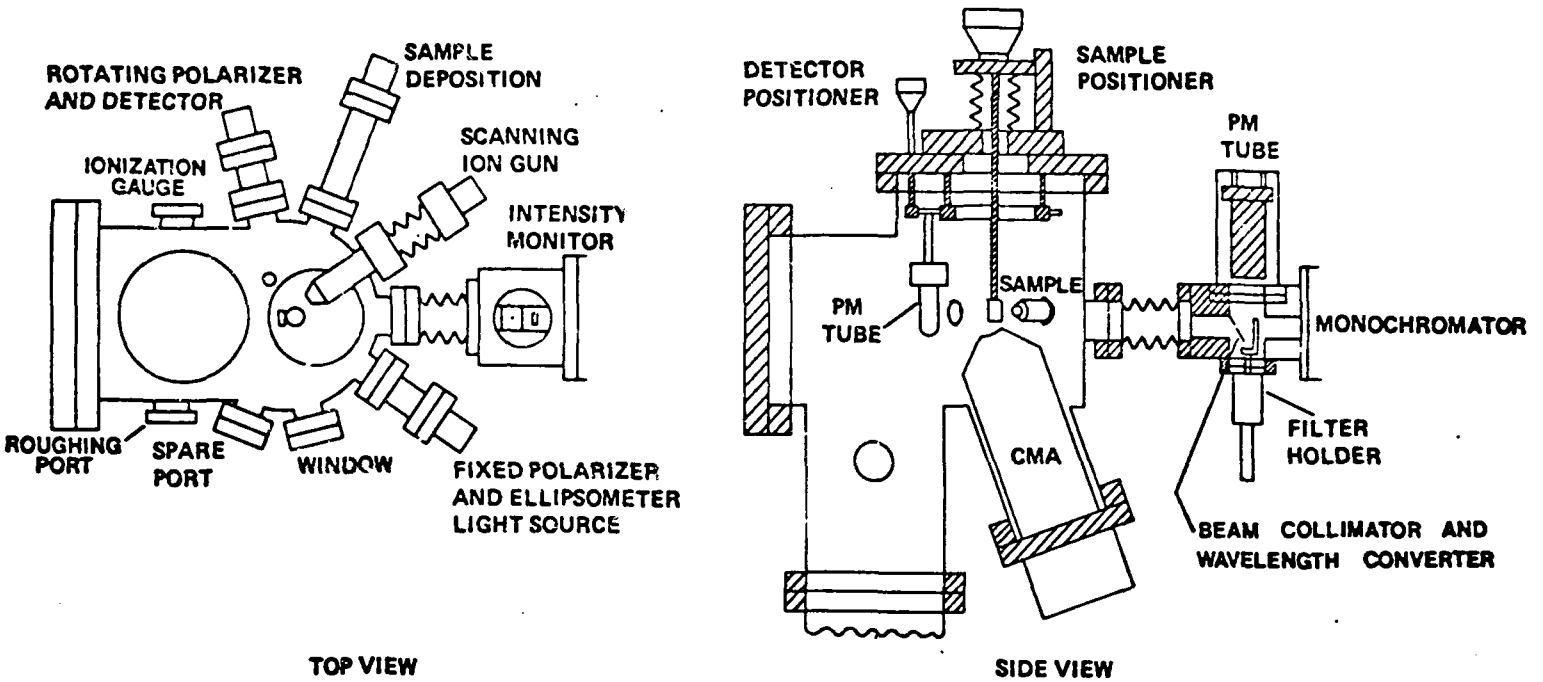

SAMPLE CHAMBER/REFLECTOMETER

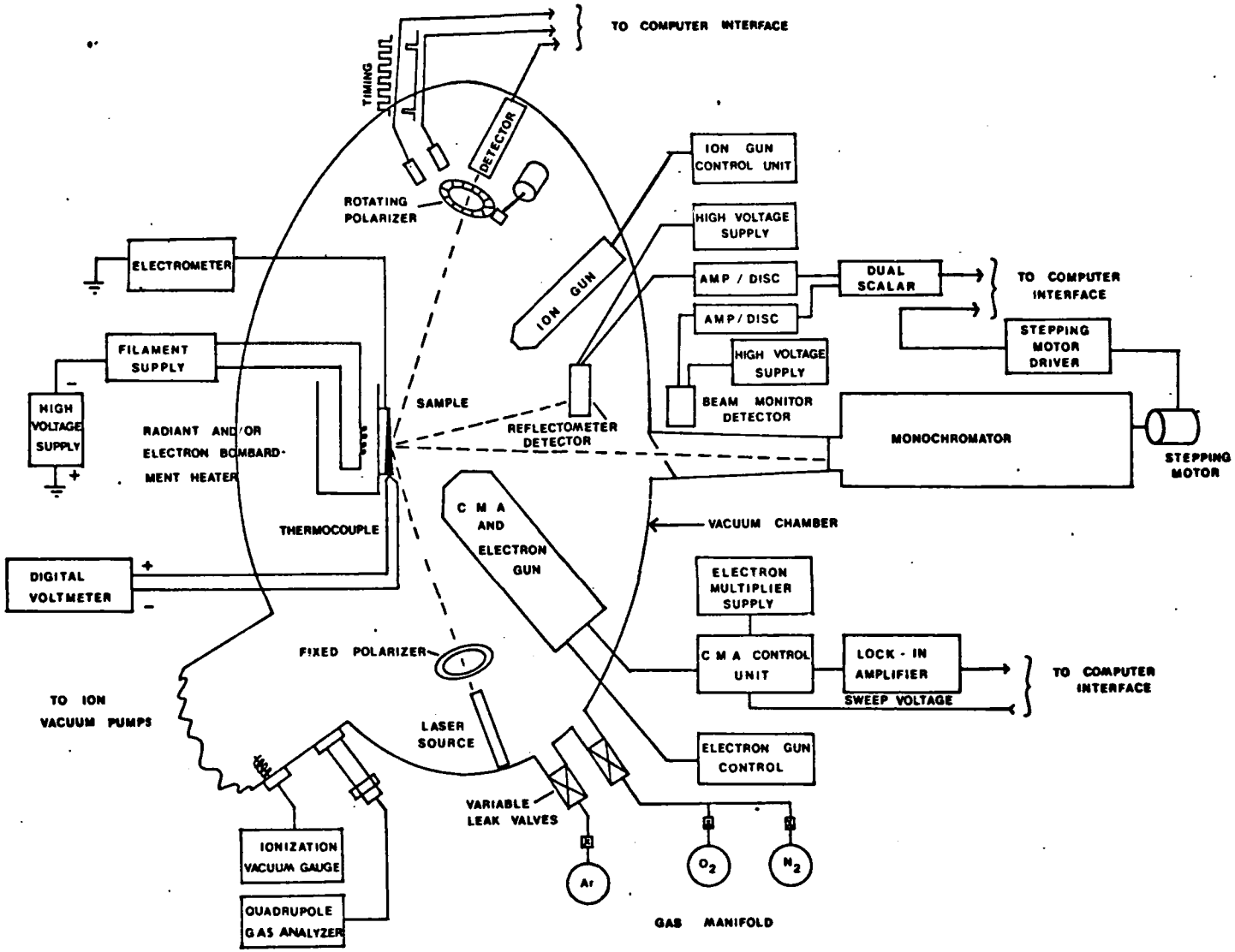

INSTRUMENTATION CONFIGURATION

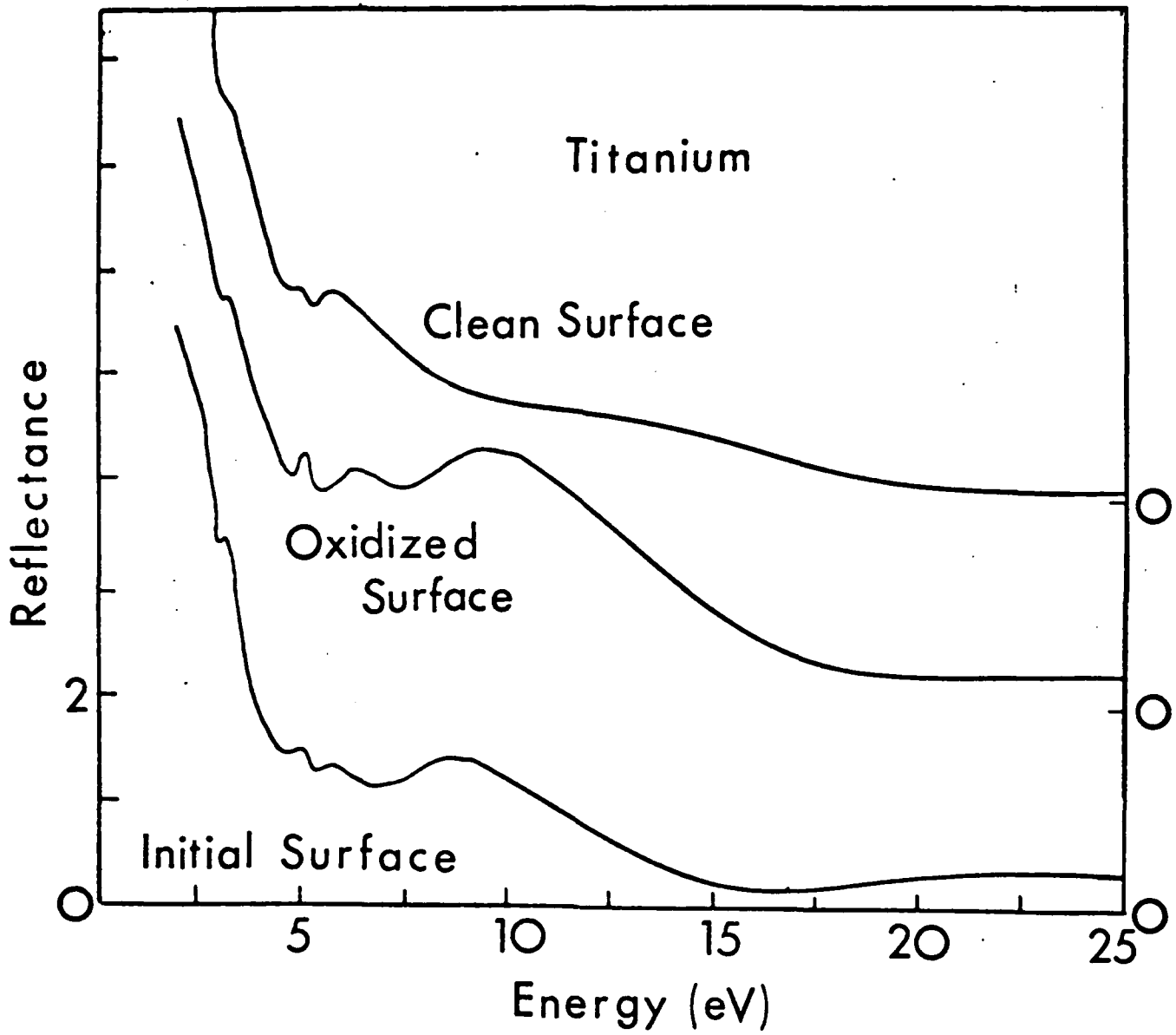
Titanium
Clean Surface
Oxidized
Surface
Initial Surface
Reflectance
0
2
5
10
15
20
25
Energy (eV)

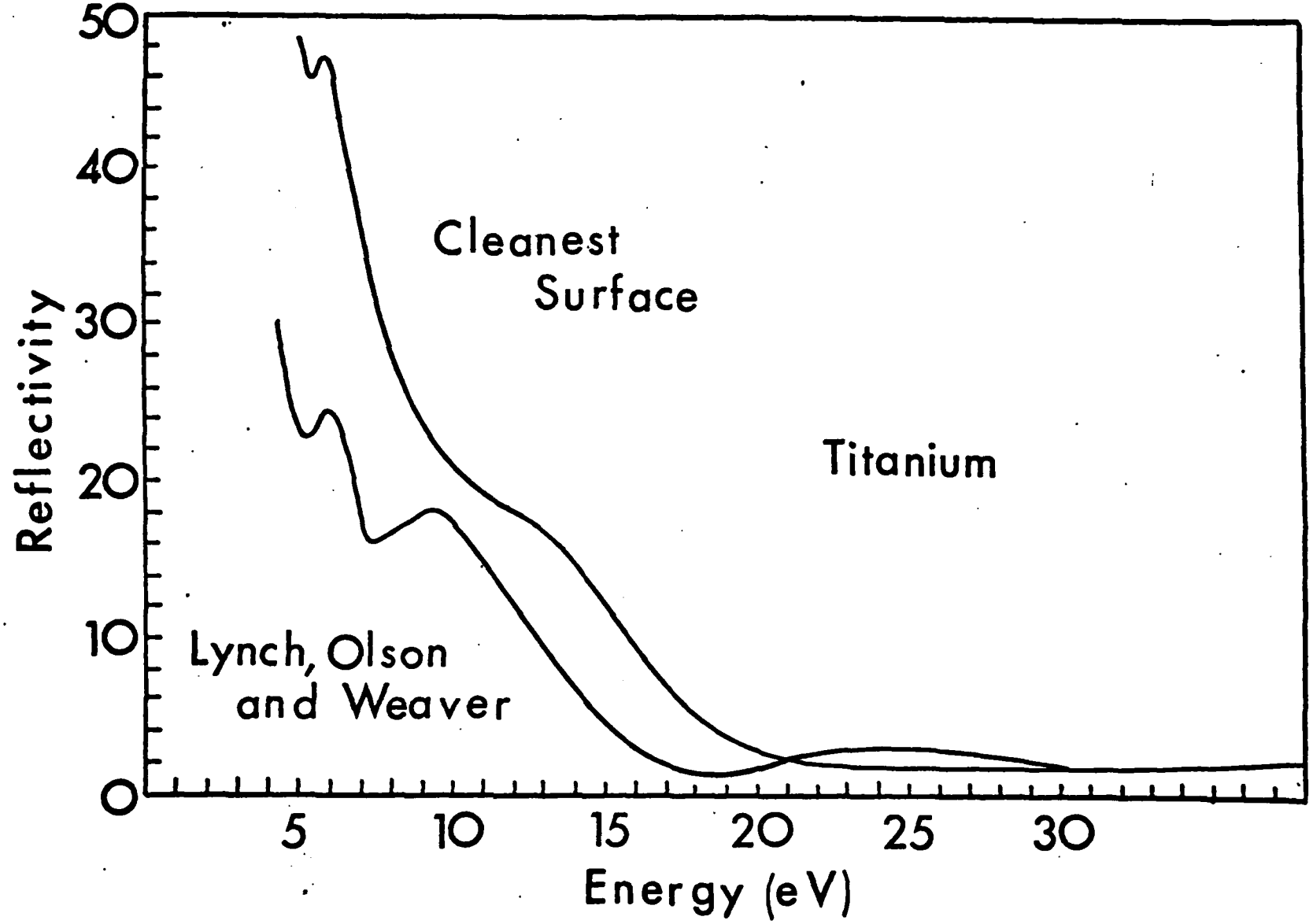
50
40
30
20
10
0
Reflectivity
Cleanest
Surface
Titanium
Lynch, Olson
and Weaver
5
10
15
20
25
30
Energy (eV)

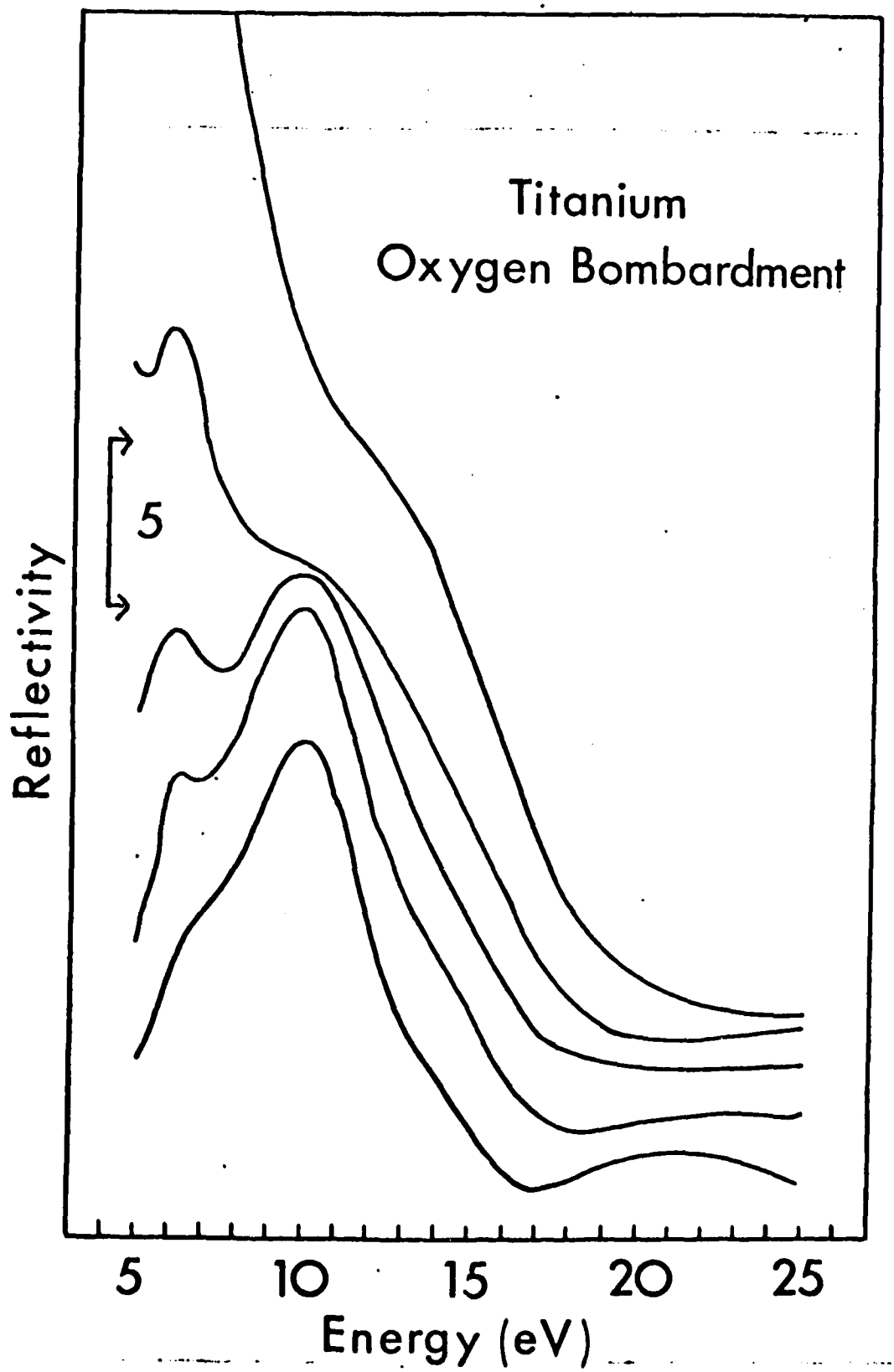
Titanium
Oxygen Bombardment
5
Reflectivity
5
10
15
20
25
Energy (eV)

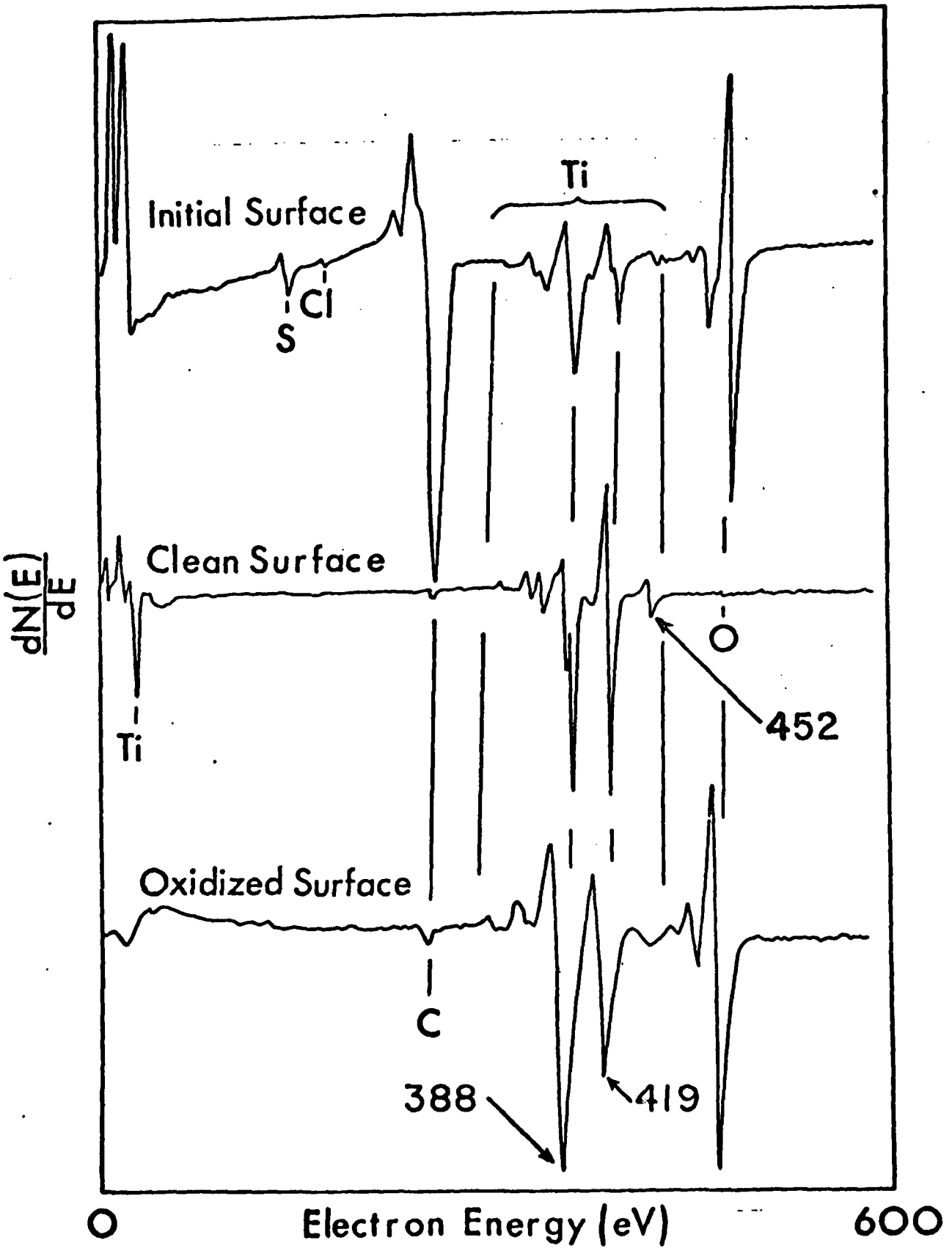
Initial Surface
Ti
S
Cl
Clean Surface
dN(E)/dE
Ti
O
452
Oxidized Surface
C
388
419
0
Electron Energy (eV)
600

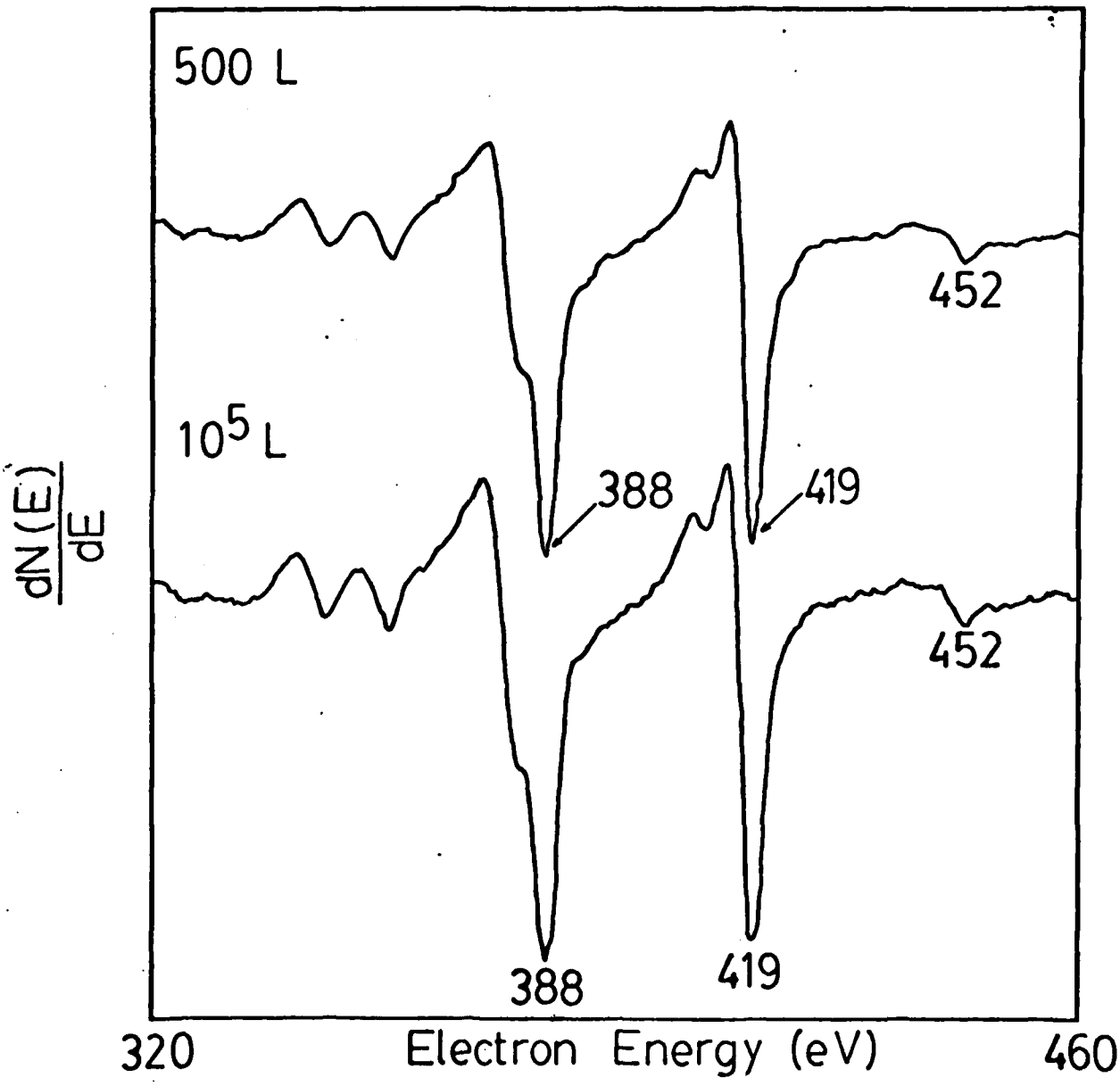
500 L
452
10^5 L
388
419
452
388
419
$\frac{dN(E)}{dE}$
320
Electron Energy (eV)
460

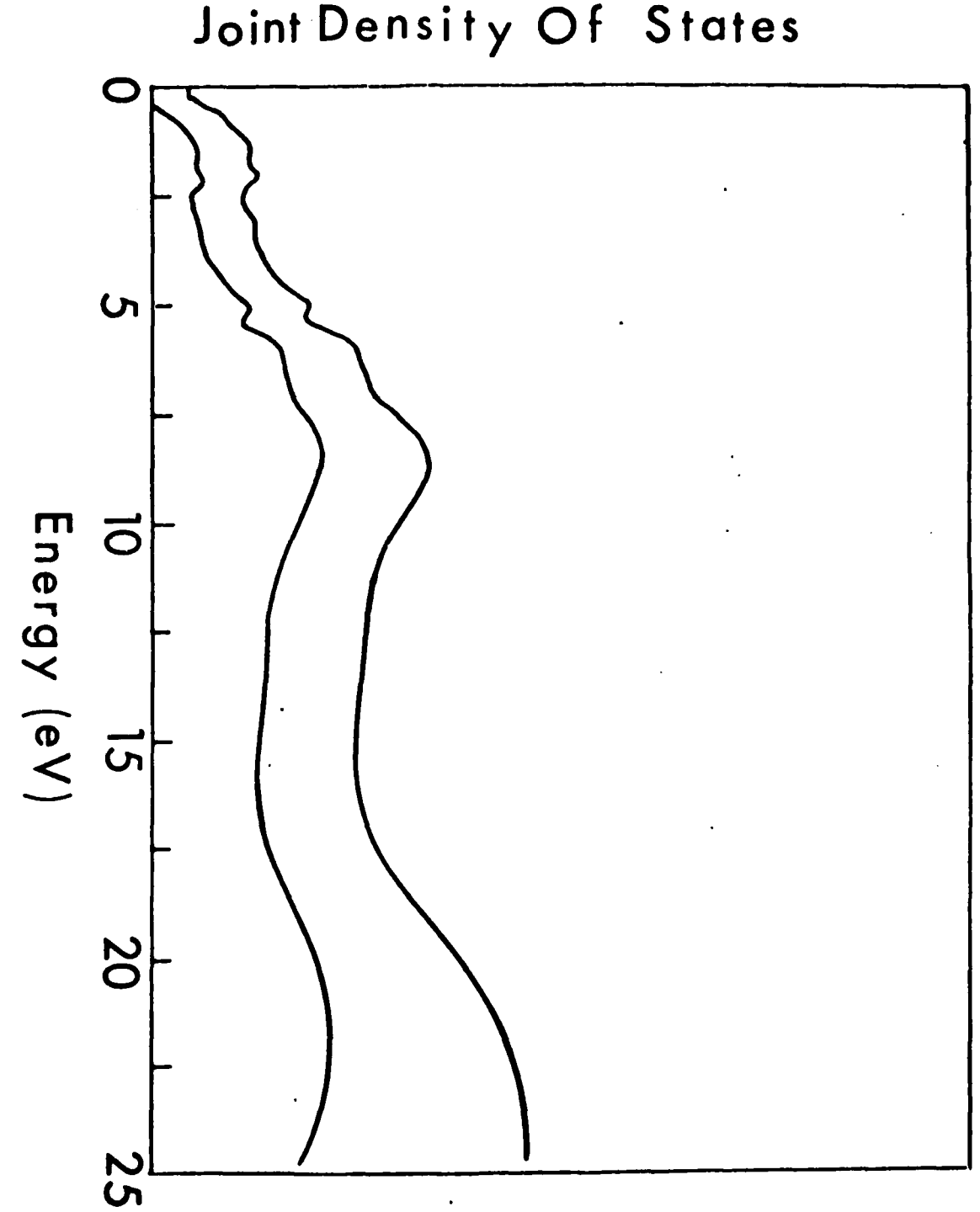
Joint Density Of States
0
5
10
15
20
25
Energy (eV)

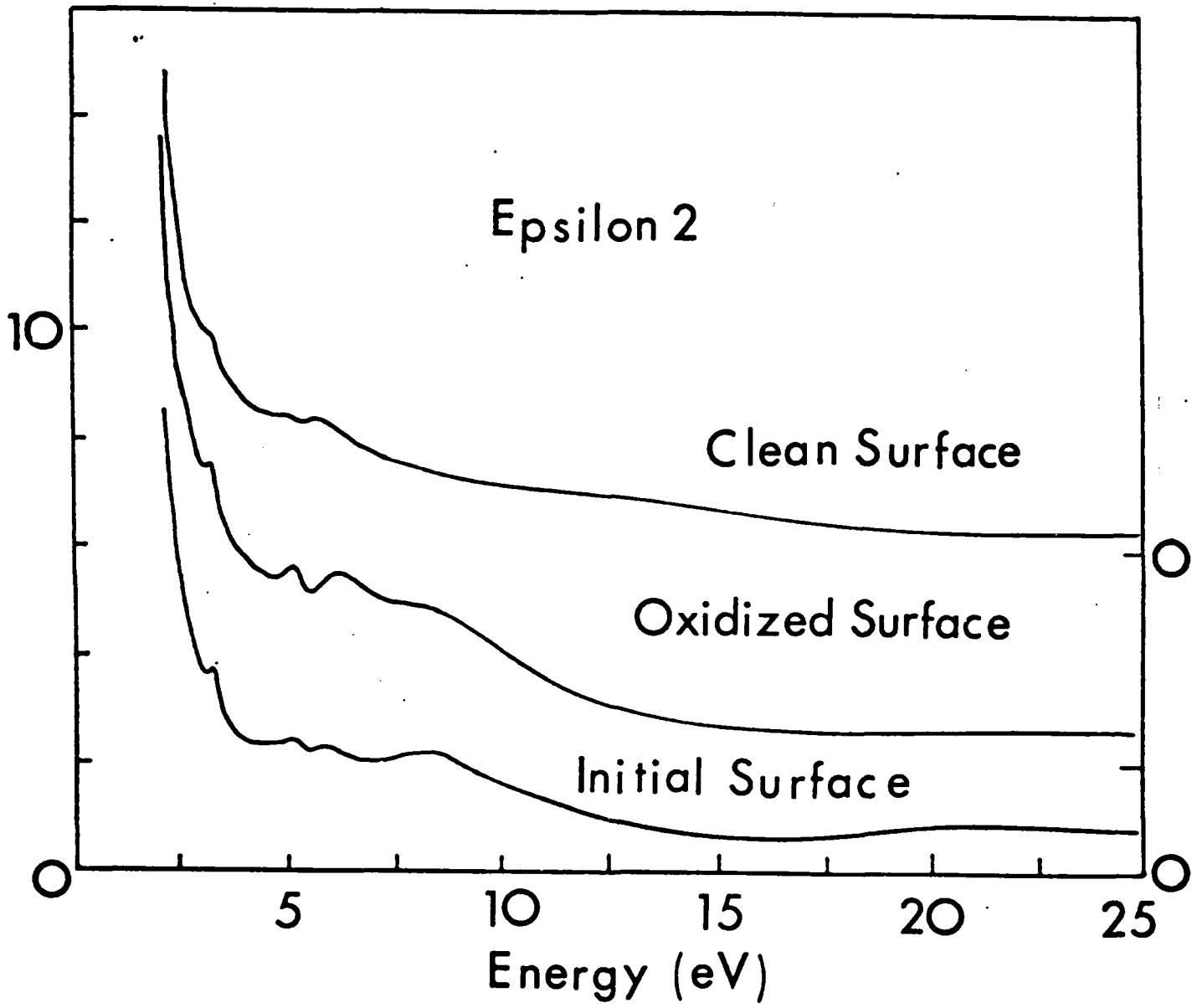
Epsilon 2
10
0
Clean Surface
Oxidized Surface
Initial Surface
0
5
10
15
20
25
Energy (eV)

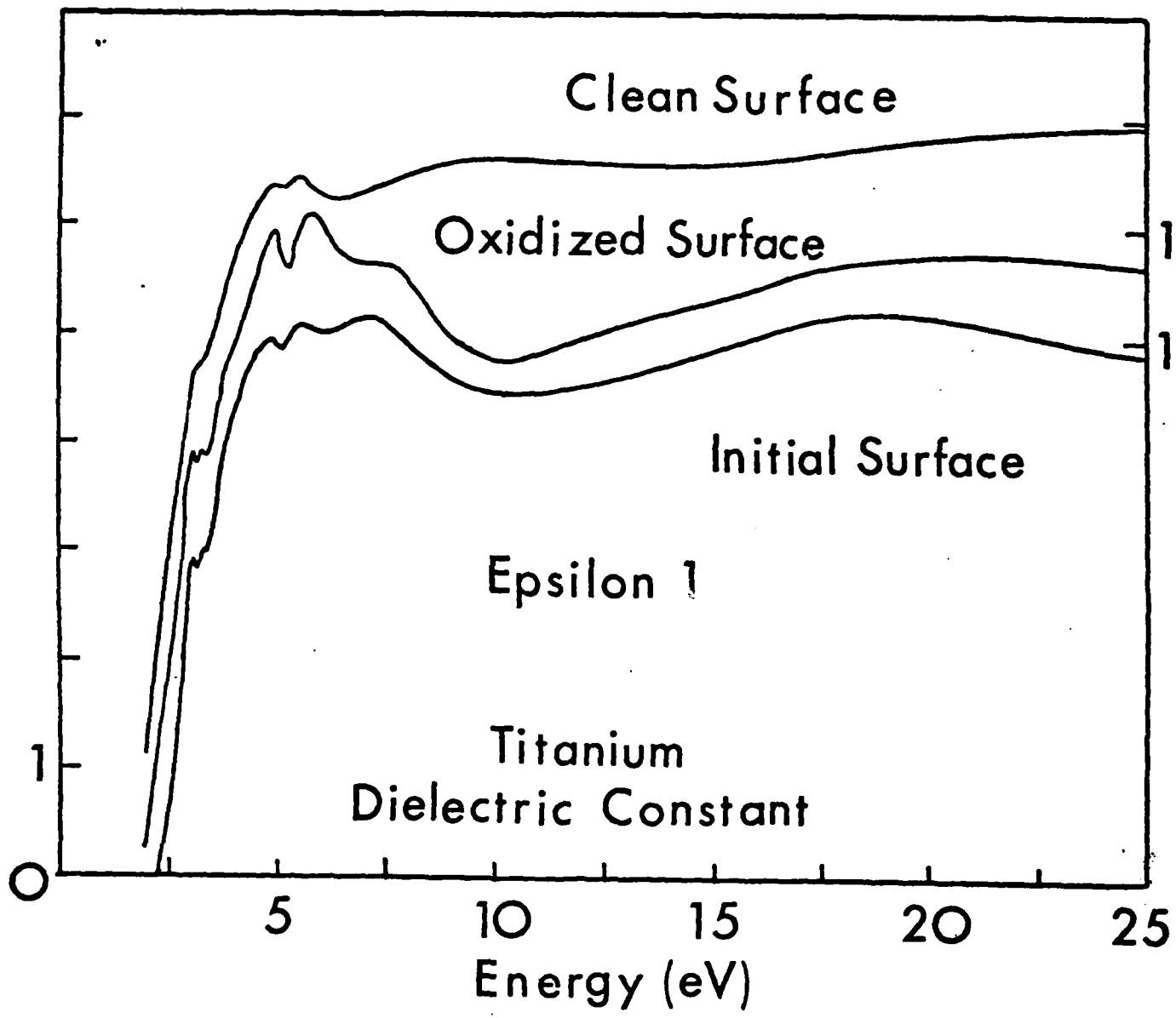
Clean Surface
Oxidized Surface
Initial Surface
Epsilon 1
Titanium
Dielectric Constant
1
1
1
0
5
10
15
20
25
Energy (eV)